FISEVIER

Contents lists available at ScienceDirect

Palaeogeography, Palaeoclimatology, Palaeoecology

journal homepage: www.elsevier.com/locate/palaeo



Late Miocene to Early Pliocene paleoceanographic evolution of the Central South Pacific: A deep-sea benthic foraminiferal perspective

Sunil K. Das ^a, N. Mahanta ^a, B. Sahoo ^a, Raj K. Singh ^{a,*}, Carlos A. Alvarez Zarikian ^b, Manish Tiwari ^c, Nishant Vats ^{a,1}, Nihal ^a, Frank Lamy ^{d,e}, Gisela Winckler ^f, Jennifer L. Middleton ^f, Helge W. Arz ^g, Julia Gottschalk ^h, Chandranath Basak ⁱ, Anieke Brombacher ^j, Oliver M. Esper ^d, Jesse R. Farmer ^k, Lisa C. Herbert ^l, Shinya Iwasaki ^m, Lester Lembke-Jene ^d, Vera J. Lawson ⁿ, Li Lo ^o, Elisa Malinverno ^p, Elisabeth Michel ^q, Simone Moretti ^r, Christopher M. Moy ^s, Ana Christina Ravelo ^t, Christina R. Riesselman ^s, Mariem Saavedra-Pellitero ^u, Inah Seo ^v, Rebecca A. Smith ^w, Alexandre L. Souza ^x, Joseph S. Stoner ^y, Igor Venancio M.P. de Oliveira ^z, Sui Wan ^{aa}, Xiangyu Zhao ^{ab}

- ^a School of Earth, Ocean and Climate Sciences, Indian Institute of Technology Bhubaneswar, Argul, Jatni 752050, India
- b International Ocean Discovery Program, Texas A&M University, College Station, United States
- ^c National Centre for Polar and Ocean Research, Ministry of Earth Sciences, Vasco-da-Gama 403804, Goa, India
- ^d Alfred Wegener Institute, Helmholtz-Center for Polar and Marine Research, Bremerhaven, Germany
- ^e MARUM–Center for Marine Environmental Sciences, Bremen, Germany
- f Lamont-Doherty Earth Observatory, Columbia University, NY, USA
- ^g Leibniz Institute for Baltic Sea Research, Warnemünde, Germany
- ^h University of Kiel, Germany
- ⁱ Department of Earth Sciences, University of Delaware, USA
- ^j Department of Earth & Planetary Sciences, Yale University, USA
- k Department of Geosciences, Princeton University, USA
- ¹ School of Marine and Atmospheric Sciences, Stony Brook University, USA
- ^m Graduate School of Environmental Science, Hokkaido University
- ⁿ Department of Earth and Planetary Sciences, Rutgers, The State University of New Jersey, USA
- Department of Geosciences, National Taiwan University, Taiwan
- ^p Department of Earth and Environmental Sciences, University of Milano-Bicocca, Italy
- q Laboratoire des Sciences du Climat et de l'Environnement LSCE. Institut Pierre Simon Laplace IPSL. CNRS-CEA-UVSO. France
- ^r Climate Geochemistry Department, Max Planck Institute for Chemistry (MPIC), Germany
- ^s Geology Department, University of Otago, New Zealand
- ^t Ocean Sciences Department, University of California, Santa Cruz, USA
- ^u School of Geography, Earth and Environmental Sciences, University of Birmingham, United Kingdom
- V Global Ocean Research Center, Korea Institute of Ocean Science and Technology (KIOST), Republic of Korea
- w Department of Geosciences, University of Massachusetts-Amherst, USA
- x Department of Geology, Federal University of Rio de Janeiro, Brazil
- y College of Earth, Ocean and Atmospheric Sciences, Oregon State University, USA
- ² Postgraduate Program in Geochemistry, Department of Geochemistry, Fluminense Federal University, Niterói, Rio de Janeiro, Brazil
- ^{aa} South China Sea Institute of Oceanology, Chinese Academy of Sciences, China
- ab National Institute of Polar Research, Geoscience Group, Japan

A R T I C L E I N F O

Editor: M Elliot

The bottom water conditions in the Central South Pacific (CSP) and associated changes in the Lower Circumpolar Deep Water (LCDW) and Antarctic Bottom Water (AABW) under warmer-than-present conditions need to be better understood. These water masses transfer their properties to the major ocean basins. We analyzed Late Miocene to Early Pliocene (5.6–3.6 Ma) marine sediment core sections from the CSP for benthic foraminifera, ice

E-mail address: rksingh@iitbbs.ac.in (R.K. Singh).

https://doi.org/10.1016/j.palaeo.2024.112252

 $^{^{\}ast}$ Corresponding author.

Current Address: Department of Applied Geology, Indian Institute of Technology (Indian School of Mines), Dhanbad, India.

Antarctic Circumpolar Current Lower Circumpolar Deep Water Productivity Antarctic Bottom Water Southern Ocean Benthic foraminifera Ostracoda rafted debris (IRD), Ostracoda, planktic foraminifera *Orbulina universa* abundance, and organic geochemical proxies to assess the bottom water characteristics under warmer-than-present day conditions. A significant increase in IRD abundance between 5.3 and 4.9 Ma marks the Early Pliocene warm phase. The benthic foraminiferal assemblages indicate shifts in bottom water conditions over time in the CSP region. Between 5.6 and 5.3 Ma, predominantly oxygenated bottom water with moderate organic matter flux prevailed. This shifted to suboxic conditions with increased organic matter flux from 5.3 to 4.9 Ma. Subsequently, between 4.9 and 4.4 Ma, bottom water conditions alternated frequently between oxic and suboxic states. Enhanced bottom water formation and inflow of LCDW and AABW in the CSP during 4.4–4.0 Ma promoted oxygenated conditions, accompanied by low organic export flux. However, sluggish bottom water circulation from 4.0 to 3.6 Ma reverted to suboxic conditions, associated with increased carbon burial. Notably, productivity peaked intermittently between 5.3 and 3.6 Ma, as indicated by the occurrence of suboxic species assemblages and increase in the abundance of *Orbulina universa*, benthic microfauna (ostracods), and other paleoproductivity indicators.

1. Introduction

The Late Miocene to Pliocene period was a geologically recent interval of Earth's climate history when global climate was generally warmer and atmospheric CO2 levels were, for the last time, either similar to or higher than today's (Steinthorsdottir et al., 2021). For instance, during the Early Pliocene Warm Period, annual mean temperatures were 2-3 °C higher than during the pre-industrial times (Prescott et al., 2019). Earth's climate history from the Late Miocene to Middle Pleistocene was marked by several episodes of global climate reorganizations, including changes in ice volume and ocean circulation (Karas et al., 2011, 2019). The temporal evolution of the Southern Ocean is tightly linked to the dynamics of the Antarctic Circumpolar Current (ACC), which connects all the major ocean basins. The ACC also plays a crucial role in the global Meridional Overturning Circulation (MOC) through the upwelling and formation of new water masses, like Antarctic Bottom Water (AABW), Circumpolar Deepwater (CDW), and the Antarctic Intermediate Water (AAIW). Thus providing a direct hydrographic link to the vast deep ocean reservoir of dissolved inorganic carbon (Kuhlbrodt et al., 2007; Lamy et al., 2019). Various studies have suggested that variations in the bottom water current strength during glacial-interglacial periods strongly influenced the paleoceanographic and paleoclimatic changes, thus impacting the global climate (Mackensen, 2004; Marshall and Speer, 2012; Wu et al., 2021). In addition, the Southern Ocean is important for the utilization of biological nutrients and the regulation of the preformed nutrient inventory for large parts of the deep ocean (Sigman et al., 2010).

Benthic foraminifera assemblages are one of the most reliable biological proxies to assess deep water characteristics because of their great sensitivity to ambient environmental parameters, such as temperature, salinity, the amount of dissolved oxygen in seawater, organic matter flux, and substrate (Gupta and Thomas, 2003; Singh and Gupta, 2010; Verma et al., 2013; Das et al., 2018, 2021; Singh et al., 2021; Vats et al., 2021; Thena et al., 2021). The quality and quantity of food and deep-sea oxygenation, influence the distribution and abundance of benthic foraminifera (Jorissen et al., 1995; Olóriz et al., 2012; Singh et al., 2021). The climatic and oceanographic changes associated with the opening and closing of the ocean basins, which took place during the Pliocene, were also assessed using benthic foraminiferal assemblages (McKay et al., 2012; Karas et al., 2019). There are very limited studies of Central South Pacific paleoceanography using benthic foraminiferal proxies (Winckler et al., 2021). The productivity variability in the Southern Ocean since the Pliocene is limited to Atlantic and Indian sectors of the Southern Ocean (Pahnke and Zahn, 2005; Karas et al., 2011, 2019; Tapia et al., 2021). However, recent publications based on International Ocean Discovery Program (IODP) expeditions 379, 382 and 383 (Gohl et al., 2021; Pérez et al., 2021; Winckler et al., 2021; Gille-Petzoldt et al., 2022; Lamy et al., 2024) have provided new information about

paleoceanography and productivity changes in the Southern Ocean, but not based on benthic foraminifera. Hence, this study aims to provide the first benthic foraminiferal record covering the Late Miocene to Early Pliocene from the CSP to assess deep water characteristics, with a particular focus on paleoceanographic and productivity variations during the Early Pliocene period.

2. Oceanographic setting and study area

2.1. Oceanographic setting

The Southern Ocean significantly impacts the global ocean circulation and climate. The majority of the world's abyssal and deep waters are newly formed or significantly modified in the Southern Ocean, which controls large parts of the global Meridional Overturning Circulation (Kennett, 1977; Barker and Burrell, 1977; Marshall and Speer, 2012; Talley, 2013; Carter et al., 2022). The cold, dense water sinks to abyssal depths around Antarctica's margin before travelling northwards via deep western boundary currents into the Atlantic, Indian, and Pacific oceans (Stommel, 1958; Warren, 1981; Carter et al., 2008, 2022). These extremely cold waters from the ocean's depths are brought to the surface by the process of slow upwelling (Carter et al., 2022) and contribute to the warm surface circulation across all the ocean basins. The formation of Subantarctic Mode Water (SAMW) is caused by the mixing of the surface waters, north of the Subantarctic Front (Rintoul et al., 2001; Sloyan and Rintoul, 2001; Herraiz-Borreguero and Rintoul, 2011). Generally, SAMW is well-oxygenated and sinks to a depth of ~500 m (Fig. 1b). AAIW reaches a maximum depth of ~1400 m beneath SAMW (Fig. 1b). It is characterized by a salinity minimum (34.3–34.5) (Fig. 1b), which distinguishes AAIW from other water masses at equivalent depths (Rintoul et al., 2001). CDW dominates the Southern Ocean in terms of volume, and it ranges from \sim 1400 to \sim 3600 m (Fig. 1b). The deep Pacific basin is primarily fed by CDW. The CDW can be distinguished as Lower Circumpolar Deep Water (LCDW) and Upper Circumpolar Deep Water (UCDW) (Sloyan and Rintoul, 2001). Oxygen minimum and elevated nutrient concentrations mark the presence of UCDW, and it has a depth range of 1400-2500 m (Fig. 1b). LCDW is characterized by a salinity maximum between 34.70 and 34.75, and it has a depth range of 2500-3600 m (Fig. 1b; Orsi et al., 1995; Carter et al., 2008; Toyos et al., 2020). Intense turbulent mixing around topographic features in the deep Southern Ocean increased the quantity of "carbon-rich" subsurface water integrated into LCDW (from UCDW above and AABW below) and exported northwards to the Atlantic and Indo-Pacific region (Orsi et al., 1999; Kawabe and Fujio, 2010; Jiang et al., 2020). The Ross Sea and the Weddell Sea are considered to be the most important source of AABW (Orsi et al., 2002; Orsi and Wiederwohl, 2009; Kerr et al., 2018;) having a density $> 28.27 \text{ kg m}^{-3}$ and found at great depths (down to 6000 m) because of their higher density (Orsi et al., 1999).

2.2. Study area

The IODP Expedition 383, Site U1541 (54°12.756'S, 125°25.540'W) was drilled at 3604 m water depth from the seafloor to basement, and recovered a ~ 146 m thick sedimentary sequence extending back to the Late Miocene (Winckler et al., 2021). At Site U1541 three holes were drilled using the JOIDES Resolution advanced piston corer and recovery was above 100% (Winckler et al., 2021). Site U1541 is located within the path of the Subantarctic-Antarctic Circumpolar Current (SACC), 100 nmi north of the modern mean position of the Subantarctic Front (SAF). The associated fronts in this ACC sector are strongly influenced by the topography of the seafloor spreading systems (Udintsev and Eltanin-Tharp Fracture Zone systems) as Site U1541 is located just 160 nmi away from the western flank of East Pacific Rise (EPR) and north of the Eltanin-Tharp Fracture Zone (Fig. 1a; Winckler et al., 2021). Seasonally, sea-surface temperatures (SSTs) range from 3 (July-September) to 7 °C (January-March). In the modern ocean, Site U1541 is bathed by the LCDW (Fig. 1b) and is just above the boundary with AABW. Hence, this site is sensitive to the variability of AABW through time (Winckler et al., 2021).

3. Material and methods

3.1. Age model and sedimentation rate

We analyzed 97 sediment samples from Holes U1541B and U1541C, between 85.2 and 105.9 m core composite depth below sea floor (CCSF). These samples spanned between ~5.6 and 3.6 Ma, covering the Late Miocene to Early Pliocene interval. The major lithofacies observed is dominance of varying proportions of diatom bearing nannofossil oozes interbedded with pure nannofossil oozes (Winckler et al., 2021). The age model developed and improved by the shipboard science party through orbital tuning of the Gamma-ray attenuation (GRA)-density record to obliquity (Lamy et al., 2024) was utilized to interpolate the age of each

analyzed sample. The average time resolution between samples is $\sim \! 19$ kyr based on interpolated ages.

3.2. Sample processing for benthic foraminiferal analysis

Samples were dried, and ~ 20 g of the dry sediment samples were soaked in water for 8–12 h with 4–5 drops of H₂O₂ and wet sieved over a 63 μm sieve using a gentle shower (Das et al., 2018). The >63 μm fractions were dried in a vacuum oven at 45 °C before being transferred into glass vials with proper labeling. Adequate measures were taken to avoid any contamination. All the sieves were washed in an ultrasonicator for 15 min before each use, and methylene blue was applied to the sieve net to identify potentially contaminated specimens if any. The >63 µm fractions were dry-sieved over a 125 µm sieve, and approximately 300 benthic foraminifera specimens were picked and counted from a suitable aliquot using a stereo zoom microscope. An Otto splitter was used to get the suitable aliquot. Whole samples were analyzed if the benthic foraminiferal abundance was fewer than 300 specimens. Additionally, the size fractions between 63 and 125 µm were scanned, and it was observed that no notable infaunal, elongated, or smaller benthic foraminiferal species were present. The benthic foraminifera were identified down to genus level following Loeblich and Tappan (1988) and to species level following (Scott et al., 2000; Holbourn et al., 2013; Das et al., 2018, 2021). The species with an abundance of >7% in 7 or more samples are considered dominant species (Fig. 2) and preservation of benthic foraminifera is good except for a few selected intervals. The bottom water oxygenation condition is inferred using dominant benthic foraminifera species oxygenation preferences and benthic foraminifera species are grouped into oxic, and suboxic assemblages (Fig. 2; Table 1). Following previous approaches (e.g., Kaiho, 1994; Erdem et al., 2020; Vats et al., 2021), we refer to conditions as dysoxic when the dissolved oxygen (DO) level is between 0.1 and 0.3 ml l^{-1} , as suboxic when the DO level is between 0.3 and 1.5 ml l^{-1} , and as oxic when the DO level is $>1.5 \text{ ml l}^{-1}$.

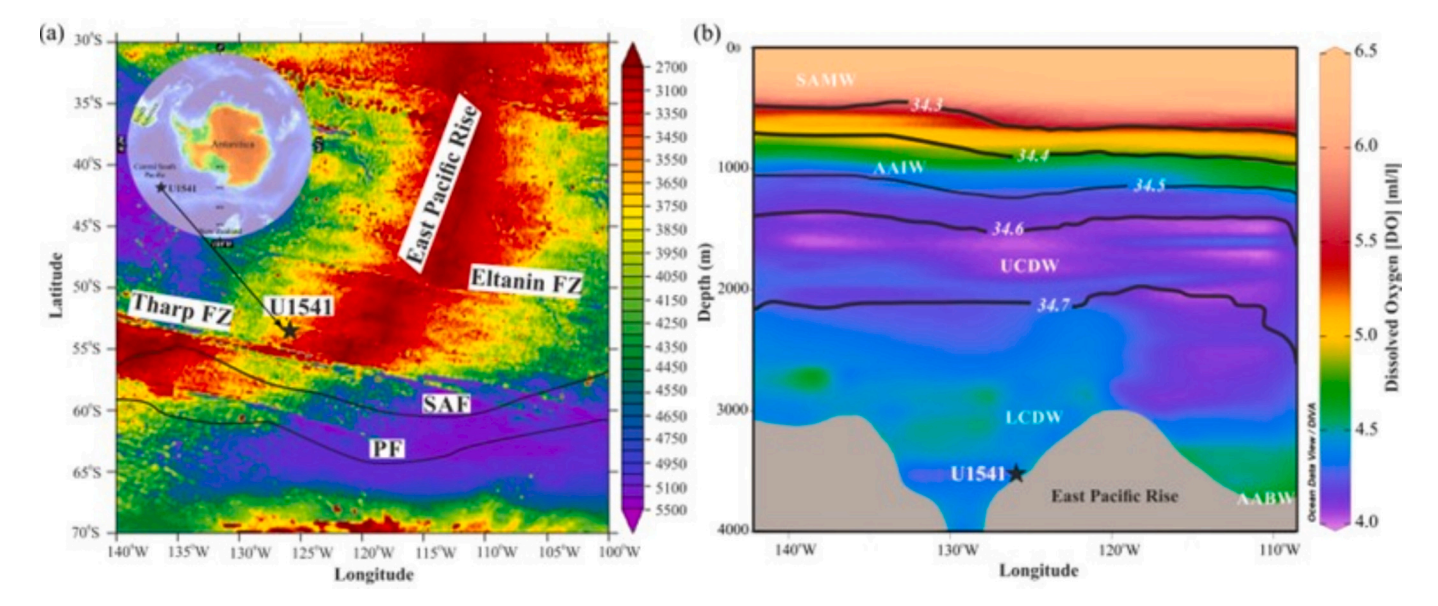


Fig. 1. (a) Location map of Site U1541 in the Central South Pacific (CSP) generated using Bathymetry/Topography – ETOPO1 Bedrock Global Relief Model [Data source: Asia Pacific Data Research Centre]. East Pacific Rise (EPR), Sub Antarctic Front (SAF), Polar Front (PF), and some fracture zones (FZ) are shown, (b) Vertical profile of Dissolved Oxygen (DO) (Garcia et al., 2013), Sea Water Salinity contours (Zweng et al., 2019) at 54.12°S (the studied Site U1541) in the Central South Pacific (CSP) are generated using Ocean Data View (ODV) software. Salinity (black lines) and oxygen (colors) distributions in the Central South Pacific are used to visualize major water masses. The right-side color bar represents the DO in ml l⁻¹. [Data source: Asia Pacific Data Research Centre, DO levels (objectively analyzed mean) taken from World Ocean Atlas 2013 at 1-degree resolution (Garcia et al., 2013), Seawater Salinity (objectively analyzed mean) is decadal average (1955–2017) of annual data accessed from World Ocean Atlas 2018 at 1-degree resolution (Zweng et al., 2019)]. The main water masses are compiled from (Orsi et al., 1995; Speer et al., 2000; Rintoul et al., 2001; Winckler et al., 2021; Carter et al., 2022). Water masses are SAMW, Subantarctic Mode Water; AAIW, Antarctic Intermediate Water; UCDW, Upper Circumpolar Deep Water; LCDW, Lower Circumpolar Deep Water; AABW, Antarctic Bottom Water.

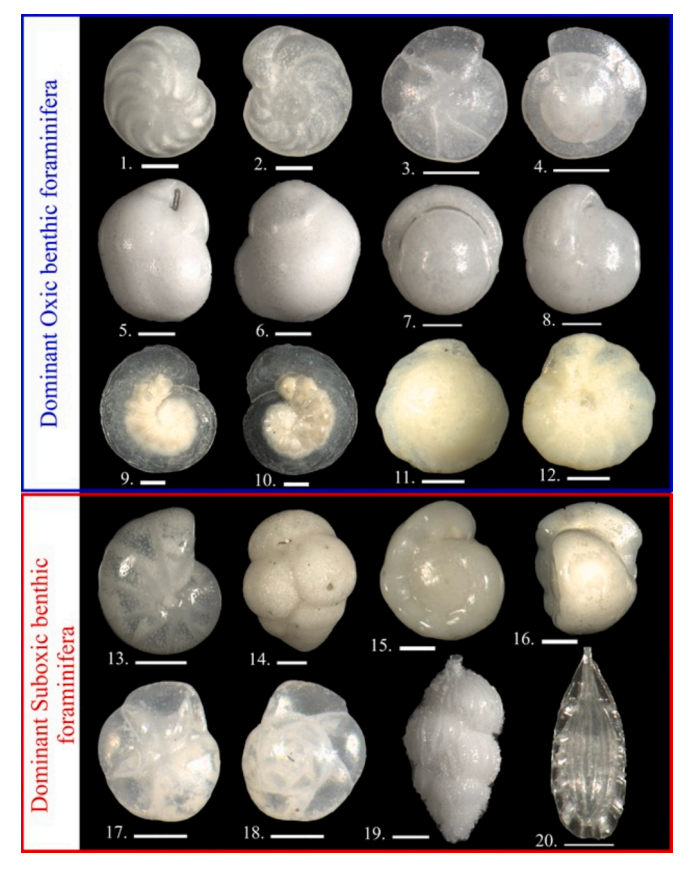


Fig. 2. Photomicrographs of dominant oxic and suboxic species at Site U1541, Central South Pacific. White bar indicates scale = 100 μm. The oxic species are: 1. Cibicidoides wuellerstorfi (umbilical view), 2. Cibicidoides wuellerstorfi (spiral view), 3. Oridorsalis umbonatus (umbilical view), 4. Oridorsalis umbonatus (spiral view), 5. Globocassidulina subglobosa (umbilical view), 6. Globocassidulina subglobosa (spiral view), 7. Pullenia bulloides (apertural view), 8. Pullenia bulloides (side view), 9, 10. Laticarinina pauperata (side view), 11. Nuttallides umbonifera (spiral view), 12. Nuttallides umbonifera (umbilical view), 13. Melonis affinis (side view), 14. Eggerella bradyi (side view), 15. Gyroidina soldanii (spiral view), 16. Gyroidina soldanii (side view), 17. Epistominella exigua (umbilical view), 18. Epistominella exigua (spiral view), 19. Uvigerina peregrina (side view), 20. Fissurina striolata (side view).

We also counted ice rafted debris (IRD), the planktic foraminifera Orbulina universa, and the number of Ostracoda valves in $>\!125~\mu m$ size fractions from the same split that was used for benthic foraminifera analysis. All abundance data are reported in per gram dry sediment. Since Site U1541 is located far from any continents, transporting larger grains (>125 μm) to its location is not conceivable, hence we have interpreted lithic sediments as IRD.

3.3. Benthic foraminiferal accumulation rates and paleoproductivity

Benthic Foraminiferal Accumulation Rate (BFAR, g cm⁻² kyr⁻¹) was calculated by multiplying the number of benthic foraminifera per gram of dry sediment by the Linear Sedimentation Rate (LSR, cm kyr⁻¹) and the dry bulk density (DBD, g cm⁻³) (Herguera and Berger, 1991; Gastaldello et al., 2023, Eq. (1)). The age model utilized a straightforward linear sedimentation rate (LSR) computation between age-depth control points. The DBD was interpolated from measurements of moisture and density (MAD) samples taken during Expedition 383 (Winckler et al., 2021).

Table 1

Species

Classification of bottom-water dissolved oxygen ($[O_2]_{BW}$) thresholds using benthic foraminifera oxygenation preferences in general. Environmental preferences of dominant species, which present $\geq 7\%$ in 7 or more samples at Site U1541 are discussed. These species are grouped as oxic, and suboxic assemblages based on their environmental preferences.

Environmental

References

Microhabitat

		preferences	
Oxic Species, (>1 Cibicidoides spp.	.5 ml l ⁻¹), Kaiho (Epifaunal	1994); Erdem et al. (2020); Strong bottom currents and low flux of organic carbon, associated with NADW and AABW	Mackensen et al., 1995; Pérez- Asensio et al., 2017; Vats et al., 2021; Singh
Globocassidulina subglobosa		Cosmopolitan species, prefers well-oxygenated deep	et al., 2021 Gupta et al., 2004; Verma et al., 2013; de
		waters with intermediate to strong food supply, associated	Araújo et al., 2018; Vats et al., 2021; Singh
		with the NADW and AABW	et al., 2021
Laticarinina pauperata		Indicator of deep southern source water like AABW, found in cold, well-oxygenated deep water with a	Bhaumik et al., 2007; Singh et al., 2012, 2021
Nuttallides umbonifera		fluctuating flux of organic materials Prefers cold, corrosive, oligotrophic, high	Singh and Gupta, 2004; Singh
шиопцега		oxygen levels, indicative of AABW	et al., 2012, 2021
Oridorsalis umbonatus	Epifaunal to shallow infaunal	Cosmopolitan species can survive food- limited conditions, well-oxygenated, low- organic carbon flux	Takata et al., 2019; Vats et al., 2021
Pullenia spp.		Intermediate flux of organic matter in well-oxygenated deep waters of AABW	Singh and Gupta, 2004; Verma et al., 2013
Suboxic Species,	(0.3–1.5 ml l ⁻¹), K	aiho (1994); Erdem et al. (2	2020); Vats et al.
Eggerella bradyi	Shallow to deep Infaunal	Preferences is not well constrained; it may withstand low oxygen conditions	Bhaumik et al., 2007; De and Gupta, 2010; Thena et al., 2021
Fissurina spp.		Indicative of low oxygen conditions and restricted phytodetritus input	Morigi, 2009; Das et al., 2017
Melonis spp.		Associated with degraded refractory organic matter with varied oxygenation conditions	Thena et al., 2021; Vats et al., 2021
Uvigerina spp.		Oxygen-depleted environments, high sustained flux of organic matter	Gallagher et al., 2018; Das et al., 2018, 2021
Epistominella exigua	Epifaunal	Opportunistic species exhibits seasonal phytodetritus input	Jorissen et al., 2007; De and Gupta, 2010; Kaithwar et al.,
0 11			2020

Dysoxic species, (0.1–0.3 ml l⁻¹), Kaiho (1994); Erdem et al. (2020); Vats et al. (2021).

Low oxygen conditions,

moderate organic flux

Gupta et al.,

et al., 2017;

2006; De and

Gupta, 2010; Das

Thena et al., 2021

This study did not find any distinct dysoxic species that are dominant at this site.

Gyroidina spp.

$$BFAR = \text{no.of benthic for a minifer a } \left(g^{-1}\right) \times LSR \left(\text{cm kyr}^{-1}\right) \times DBD \left(g \text{ cm}^{-3}\right) \left[g \text{ cm}^{-2} \text{ kyr}^{-1}\right]$$

$$\tag{1}$$

Herguera (2000) obtains a simple equation that links "paleo" primary productivity (PP, gC cm⁻² kyr⁻¹) to BFAR (Eq. (2)).

$$PP = 0.4 \text{ x } Z_{km} \text{ x (BFAR)}^{0.5}$$
 (2)

where Z is water depth in kilometers.

The flux of organic matter (J_{sf} , gC cm⁻² kyr⁻¹) to the sea-floor is calculated as (Eq. (3); Herguera, 2000),

$$J_{sf} = 6.5 \text{ x (BFAR)}^{0.64} \tag{3}$$

Particle export efficiency (PE $_{eff}$) measures the percentage of primary production exported from the surface ocean to 100 m depth (Henson et al., 2012). The proportion of exported organic matter from 100 m level to the deep ocean (\sim 2000 m) is known as transfer efficiency (T $_{eff}$) (Henson et al., 2012). Herguera (2000) shows that benthic organic carbon flux and BFAR from core top sediments from the equatorial Pacific and Atlantic are well-correlated. The organic matter flux on the ocean floor (J $_{sf}$) is then reconstructed using BFAR. The schematic diagram of productivity and organic flux through the ocean water column at Site U1541 is shown in Fig. 3.

3.4. Coarse fraction accumulation rates

The coarse fraction accumulation rate (CFAR) was calculated by multiplying the size fraction >63 μm wt (%) with LSR and DBD. The CFAR is frequently used as a proxy for current strength and as a rough estimate of planktonic foraminiferal accumulation rates (Diester-Haass, 1995; Gastaldello et al., 2023). In our data, the coarse fraction mostly consists of the planktic foraminifera.

CFAR = [
$$> 63 \ \mu \text{m wt (\%)} \] \ \text{x LSR (cm kyr}^{-1}) \ \text{x DBD (g cm}^{-3}) \ [\text{g cm}^{-2} \ \text{kyr}^{-1}]$$
 (4)

3.5. Spectrophotometry

During Expedition 383, the core color reflectance was measured using Section Half Multisensor Logger (SHMSL; Winckler et al., 2021).

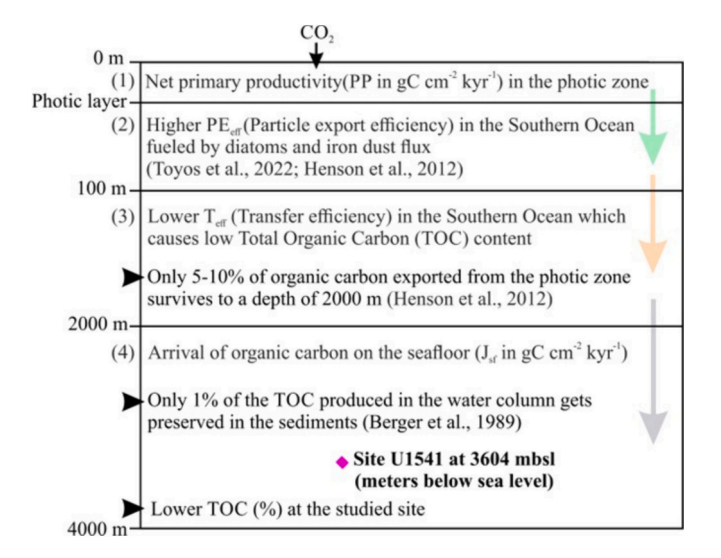


Fig. 3. Schematic diagram of productivity and organic flux through the ocean water column (not to scale, modified after Diester-Haass and Faul, 2019).

This instrument measures the reflectance of sediment surface under a standard illumination condition, and then can automatically convert and project the reflectance data into the L* and a* color space (Billmeyer and Saltzman, 1981). It has been found that color parameters L* and a* can be correlated with certain components in the sediments from a range of geological settings. For example, in sediments from oceans, the L* parameter is often proportional to the percentage of calcium carbonate (Balsam et al., 1999; Giosan et al., 2002; Liu et al., 2004; Lübbers et al., 2019); while the a* value sometimes can be related to the content of biogenic productivity (Wellner et al., 2021). In this study, we are comparing a* and L* values to support the productivity and carbonate preservation at Site U1541. The colors redness (+) and greenness (-) were provided by color reflectance a*. Greenness (-) in sediments is an indicative of more biogenic content, which may indicate better productivity in open ocean conditions (Wellner et al., 2021).

3.6. Total organic carbon, inorganic carbon, and calcium carbonate analysis

For total carbon (TC) and total organic carbon (TOC) analyses, we followed the method described in Das et al. (2021). Sediment samples weighing 60–65 mg were crushed and homogenized. Homogenized 30–35 mg of the dry sample was packed in tin foil for TC analysis using a TOC analyzer (Elementar Vario TOC Select) at the School of Earth, Ocean, and Climate Sciences, IIT Bhubaneswar. The remaining 30–35 mg of the homogenized sample was weighed in a silver boat, and a few drops of concentrated HCl were added to remove inorganic carbon. The acidified samples were dried in an oven at 105 °C for 5–6 h. The inorganic carbon-free dry sample was wrapped in tin foil along with the silver boat and analyzed for TOC. The analytical error of the instrument is within 4%. TOC was subtracted from TC to calculate total inorganic carbon (Eq. (5), TIC or C_{inorg}).

$$C_{inorg} (wt\%) = TC (wt\%) - TOC (wt\%)$$
(5)

 C_{inorg} was multiplied by 8.33 to get the total weight (%) of $CaCO_3$ in the sample (Eq. (6)).

$$CaCO_3 (wt\%) = C_{inorg} \times 8.33 (wt\%)$$
 (6)

3.7. Carbonate mass accumulation rates

Carbonate mass accumulation rates (MAR_{carbonate}; g cm⁻² kyr⁻¹) are calculated by multiplying carbonate contents (%) and MAR_{bulk} sediment (g cm⁻² kyr⁻¹). MAR_{bulk} sediment (g cm⁻² kyr⁻¹) was calculated by multiplying the LSR (cm kyr⁻¹), and DBD (g cm⁻³). For determining MAR_{carbonate}, the following equation was used following Lübbers et al. (2019):

$$MAR_{carbonate} (g cm^{-2} kyr^{-1}) = (CaCO_3\%/100) x MAR_{bulk sediment}$$
 (7)

3.8. Statistical analysis

The Principal Component Analysis (PCA) and Pearson Correlation analysis were carried out by using the FactoMiner and Factoextra package in RStudio (Lê et al., 2008) for dominant benthic foraminiferal species (Table 1; Fig. 2), TOC, CaCO $_3$, and associated productivity parameters like BFAR, PP, and J_{sf} (Table 2).

Pearson correlation matrix of the major species (\geq 7% in 7 or more sample), Cs. Cibicidoides spp., Eb: Eggerella bradyi, Ee: Epistominella exigua, Fs: Fissurina spp., Gs: Globocassidulina subglobosa, Gys: Gyroidina spp., Lp:

<i>Laticarinine</i> productivit _e	ı <i>pauperata</i> , y (PP), orga	Ms.: Melonis nic flux to th	spp., Nu: <i>Nu</i> e sea floor (J	actionining pauperata, Ms.: Melonis spp., Nu: Nutrallides umbonifera, Ou: Oridorsalis umbonatus, Ps: Pullenia spp., Us: Uvigerina spp., productivity parameter like benthic foraminifera accumulation rate (BFAR), paleo- roductivity (PP), organic flux to the sea floor (J _s), total organic carbon (TOC, %) and CaCO ₃ (%). Significant correlation coefficients are bold.	nifera, Ou: C unic carbon (Oridorsalis un TOC, %) and	thonatus, Ps: 1 CaCO ₃ (%).	Pullenia spp Significant	idorsalis umbonatus, Ps: Pullenia spp., Us: Uvigerina spp., productivit OC, %) and $CaCO_3$ (%). Significant correlation coefficients are bold	<i>na</i> spp., proc oefficients a	luctivity par re bold.	ameter like	benthic foran	ninifera aco	cumulation	rate (BFAR), paleo-
	Cs	Gs	Nu	Гр	no	Ps	Eb	Ee	Gys	Ms	Fs	Us	CaCO ₃	TOC	BFAR	ЬР	$J_{\rm sf}$
Cs	1.00																
Gs	0.32	1.00															
Nu	-0.19	-0.43	1.00														
Lp	-0.09	-0.35	0.00	1.00													
Ou	0.40	0.25	-0.13	-0.18	1.00												
Ps	0.10	0.16	-0.27	-0.11	0.09	1.00											
Eb	-0.05	-0.13	60.0	-0.22	-0.05	0.15	1.00										
Ee	-0.13	-0.16	0.02	-0.22	-0.27	0.30	0.13	1.00									
Gys	-0.28	-0.05	-0.16	-0.18	-0.20	-0.21	0.12	90.0	1.00								
Ms	0.24	0.21	-0.12	-0.09	0.04	0.55	0.04	0.22	-0.41	1.00							
Fs	0.13	0.14	-0.31	-0.33	-0.06	0.05	0.16	-0.01	0.10	80.0	1.00						
Ns	0.02	0.07	-0.35	0.11	0.00	-0.16	-0.35	-0.15	-0.09	-0.02	-0.07	1.00					
$CaCO_3$	0.12	0.32	-0.22	-0.48	-0.02	0.25	0.11	0.26	0.17	0.19	0.37	-0.14	1.00				
TOC	0.03	0.10	-0.16	-0.15	0.09	0.04	-0.01	0.05	-0.04	-0.04	-0.01	0.17	-0.10	1.00			
BFAR	0.05	0.35	-0.22	-0.40	-0.07	0.03	90.0	0.17	0.13	90.0	0.05	0.19	0.46	0.17	1.00		
PP	0.07	0.37	-0.25	-0.40	-0.07	90.0	0.07	0.19	0.10	0.12	80.0	0.17	0.51	0.12	0.99	1.00	
$J_{\rm sf}$	90.0	0.37	-0.24	-0.40	-0.07	0.05	0.07	0.18	0.11	0.10	0.07	0.18	0.50	0.14	0.99	1.00	1.00

4. Results

4.1. Benthic foraminifera, Ice-rafted debris, Orbulina universa, and Ostracoda abundance per gram sediment

The benthic foraminifera specimens of >125 µm size counts per g of dry sediment ranges between 6 and 75, with an increasing trend between 5.5 and 5.0 Ma, 4.7 and 4.4 Ma, and 4.0 and 3.7 Ma (Fig. 4a). Icerafted debris (IRD)/detrital of $>125~\mu m$ size has maximum abundance per g dry sediment between 5.5 and 4.6 Ma and has merely present at the other intervals (Fig. 4b). Planktic foraminifera Orbulina universa (>125 μm size) counts per g dry sediment is high between 5.5 and 4.6 Ma, and between 4.0 and 3.7 Ma (Fig. 4c). Ostracoda valves of >125 µm size counts in per g dry sediment peak at times when benthic foraminifera have maximum abundance between 5.6 and 4.9 Ma and between 3.9 and 3.6 Ma (Fig. 4d). Ostracoda, IRD, and Orbulina universa, had negligible abundances between 4.5 and 4.1 Ma.

4.2. Distribution of dominant benthic foraminiferal species in the Central South Pacific

The Site U1541 samples have 64 species of benthic foraminifera belonging to 45 genera. Out of 64 species identified, 12 species with an abundance of >7% in 7 or more samples are considered dominant species (Table 1; Fig. 2). The paleoecological significance of the identified dominant species are used to assess the paleoecological variability at the CSP. Further, based on their oxygenation preferences, these species are grouped into oxic, and suboxic assemblages and individual species/ genus preferred microhabitats and environmental conditions are listed in Table 1.

4.2.1. Oxic species abundance

Dominant oxic benthic foraminiferal species are Oridorsalis umbonatus, Cibicidoides spp. (includes Cibicidoides mundulus and Cibicidoides wuellerstorfi), Pullenia spp. (represented by P. bulloides, P. quadriloba, and P. quinqueloba), Laticarinina pauperata, Nuttallides umbonifera, and Globocassidulina subglobosa (Figs. 2, 5). Some of the oxic species i.e. spp. are grouped together because of their similar ecological and environmental preferences.

The abundance of Cibicidoides spp. was relatively low between 5.6 and 4.4 Ma, except for a few scattered peaks, after 4.4 Ma it increased (Fig. 5a). Oridorsalis umbonatus has a low abundance between 5.6 and 4.4 Ma, except for a few isolated peaks, and increased thereafter (Fig. 5b). Globocassidulina subglobosa abundance trend is similar to O. umbonatus and Cibicidoides spp. (Fig. 5c). Pullenia spp. shows an increasing trend from 5.4 to 4.5 Ma, followed by a decline, and subsequently, an upward trend from 3.8 Ma and onward (Fig. 5d). Laticarinina pauperata is abundant between 5.5 and 5.1 Ma, and remains consistently present between 5.1 and 4.1 Ma and declines thereafter (Fig. 5e). Nuttallides umbonifera abundance has an increasing trend between 5.2 and 4.7 Ma and a declining trend between 4.7 and 4.4 Ma and has periodic fluctuation thereafter (Fig. 5f).

4.2.2. Suboxic species abundance

Melonis spp. (M. affinis and M. pompilioides), Gyroidina spp. (mostly comprising of G. soldanii, G. cibaoensis, and G. nitida), Epistominella exigua, Eggerella bradyi, Uvigerina spp. (including mostly U. peregrina, and U. proboscidea), and Fissurina spp. (F. laevigata, F. striolata, F. formosa, F. alveolata, F. foliformis, and F. fimbriata) are the major suboxic species (Figs. 2, 6). Certain suboxic species, referred to as spp. are grouped together because of their similar ecological and environmental preferences.

Gyroidina spp. has increasing trend between 5.3 and 5.0 Ma and between 4.2 and 3.9 Ma (Fig. 6a). Eggerella bradyi has increasing trend between 5.1 and 4.8 Ma and shows a gentle increase between 4.3 and 4.0 Ma (Fig. 6b). Epistominella exigua shows overall continuous

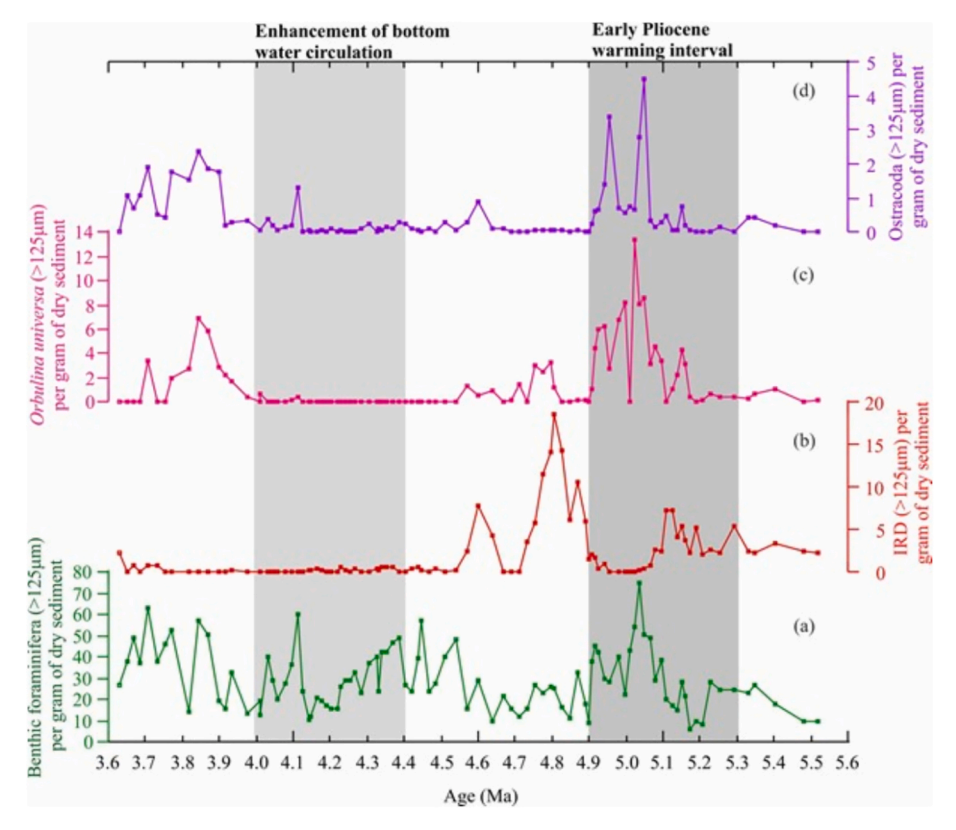


Fig. 4. (a) Benthic foraminifera (>125 μm) per g dry sediment, (b) Ice Rafted Debris (IRD, >125 μm) per g sample, (c) *Orbulina universa* (>125 μm) per g sample, (d) Ostracoda (>125 μm) per g sample, dark gray bar marks Early Pliocene warm interval, light gray bar marks enhancement of bottom water circulation.

increasing trends between 5.6 and 4.4 Ma, and then decreasing up core (Fig. 6c). *Fissurina* spp. are distributed evenly throughout the studied interval with some peaked glacial – interglacial variations (Fig. 6d). *Uvigerina* spp. sharply peaks between 5.2 and 5.0 Ma, 4.4 Ma, and 3.8 and 3.6 Ma (Fig. 6e). *Melonis* spp. increase continuously between 5.6 and 4.2 Ma, and decrease up core thereafter (Fig. 6f).

4.3. Temporal variations in carbonate preservation, total organic carbon and other productivity parameters in the CSP

The CFAR is used as a proxy for estimating planktonic foraminiferal accumulation rates (Diester-Haass, 1995; Gastaldello et al., 2023), which ranges between 0.74 and 13.4 g cm⁻² kyr⁻¹ (Fig. 7a). The color reflectance parameter a* is used as a productivity proxy and shows a similar trend with CFAR (Fig. 7b). The other color reflectance parameter L* is used as a proxy for carbonate preservation (Fig. 7c), and reflects a trend similar to $CaCO_3$ (%) and $MAR_{carbonate}$ (Fig. 7h). The benthic foraminiferal accumulation rate is one of the major productivity indicators in the deep oceans (Herguera and Berger, 1991; Herguera, 2000; Diester-Haass and Faul, 2019; Thena et al., 2021). At the Site U1541 BFAR shows high fluctuations and ranges between 3 and 71 (Fig. 7d). High BFARs are observed at ~5.2-4.9 Ma, 4.8-4.7 Ma, 4.6-4.3 Ma, 4.2-4.0 Ma and 3.9-3.6 Ma (Fig. 7d). The total organic carbon (TOC) is high during periods of high BFAR, and it ranges between 0.02 and 0.39% (Fig. 7g). The molybdenum record (U1541 XRF splice data, Winckler et al., 2021) is well matched with our TOC (%) data, which supports the interpretation of relatively higher organic carbon preservation in the sediments (Fig. 7g). CaCO3 ranges from 23.19 to 84.14% (Fig. 7h) and is higher between 5.5 and 5.3 Ma, 5.1 and 4.9 Ma, 4.6 and 4.3 Ma, and 4.1 and 3.7 Ma, while MAR carbonate ranges between 0.1 and 1.1 g cm $^{-2}$ kyr $^{-1}$ (Fig. 7h). The increase in CaCO₃ (%) and MAR_{carbonate} reflects better carbonate preservation conditions, while the decrease suggests the presence of corrosive bottom water.

4.4. Principal component analysis (PCA) and correlation analysis of major parameters

The PCA analysis shows four principal components that explain ~60% of the data variance (Table S1). The first two principal components biplot (PC1 and PC2 explain 40% of variance) together with Kmeans clustering suggest three important cluster groups, which explains three different paleoceanographic conditions associated with faunal changes, oxygenation conditions, variability in organic carbon flux, and paleoproductivity. The productivity parameters BFAR, PP, and J_{sf} are positively associated with each other and with G. subglobosa (Fig. 8; Table 2). The correlation analysis also suggests that G. subglobosa has a positive correlation with the productivity parameters, and CaCO₃ preservation (Table 2). The other species associated with this group is Cibicidoides spp., O. umbonatus, Pullenia spp., Melonis spp., and Uvigerina spp., along with TOC (%). This group suggest oxic to suboxic conditions with low to moderate productivity (Fig. 8). The contributions of Uvigerina spp. and TOC (%) are not significant within the oxic to suboxic group, however, they have a positive correlation with the productivity parameters (Table 2). The other two oxic species L. pauperata and N. umbonifera have a negative correlation with the productivity parameters and CaCO₃ (%), thus suggesting oxic corrosive bottom water conditions (Fig. 8; Table 2). The suboxic species E. exigua, E. bradyi, Gyroidina spp., and Fissurina spp. suggest suboxic high productivity as these species have a positive correlation with the productivity parameters and CaCO₃ (%) (Fig. 8; Table 2).

5. Discussion

5.1. Paleo-ecological significance of Central South Pacific

The planktic foraminifera *Orbulina universa* prefers to live in 25–100 m water depths (Hemleben et al., 1989) between $\sim\!60^{\circ}$ N and $\sim 50^{\circ}$ S

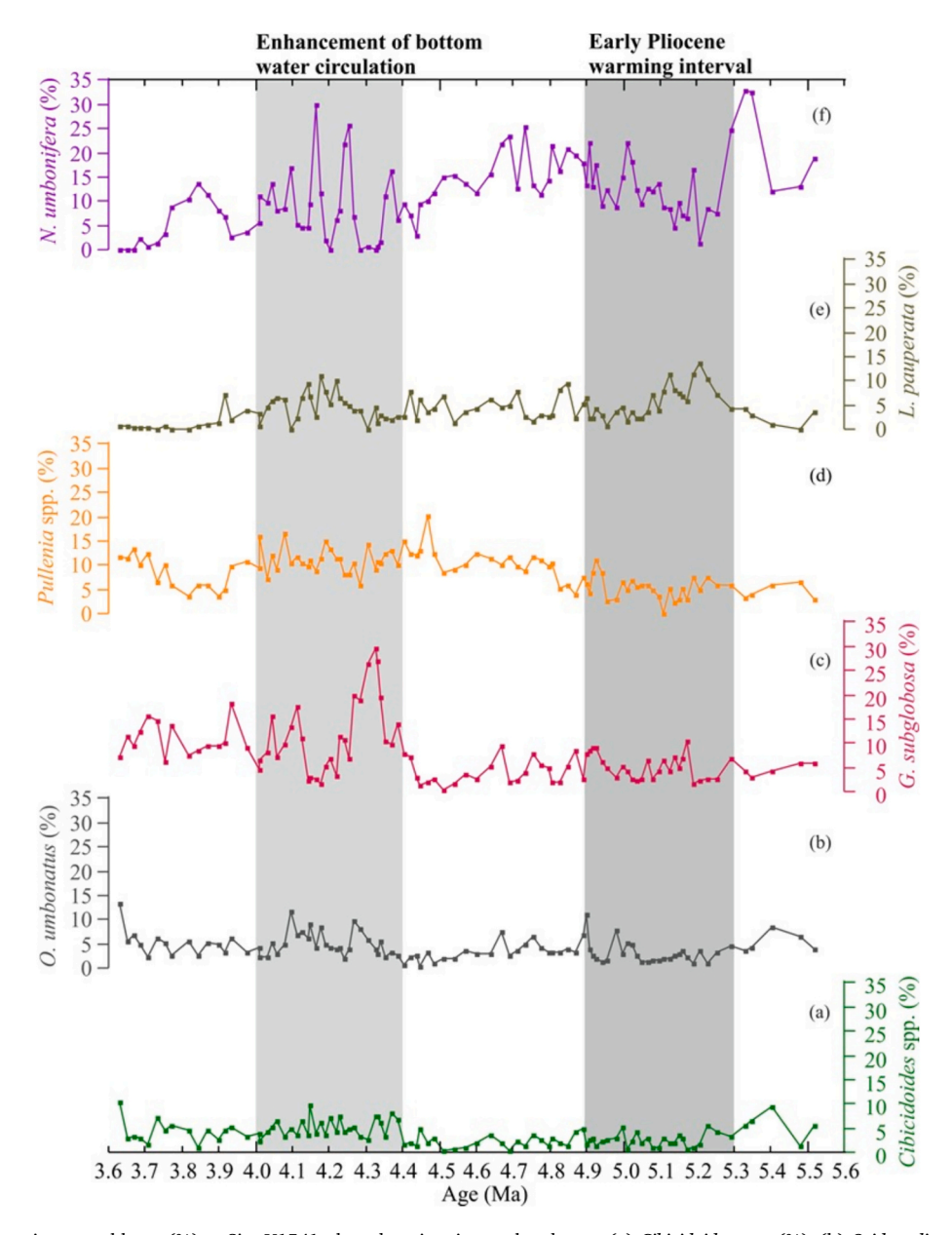


Fig. 5. Dominant oxic species assemblages (%) at Site U1541 plotted against interpolated ages, (a) Cibicidoides spp. (%), (b) Oridorsalis umbonatus (%), (c) Globocassidulina subglobosa (%), (d) Pullenia spp. (%), (e) Laticarinina pauperata (%), (f) Nuttallides umbonifera (%), dark gray bar marks Early Pliocene warm interval, light gray bar marks enhancement of bottom water circulation.

(Singh et al., 2021). This species is tolerant to temperature ranges between 9 and 30 °C and a wide range of salinity (Schiebel and Hemleben, 2017). Hence, the abundance of Orbulina universa in the >125 um size fraction suggests warmer surface water at the CSP between 5.2 and 4.9 Ma, and relatively warm between 4.0 and 3.8 Ma (Fig. 4c). The rarity of Ostracoda is reported from the deep Southern Ocean (Majoran and Dingle, 2002; Yasuhara et al., 2009). Higher abundance of Ostracoda between 5.2 and 4.9 Ma, and between 3.9 and 3.7 Ma, during times of higher surface water productivity and warm surface water temperature suggest less corrosivity at the CSP (Fig. 4d; Alvarez Zarikian, 2015). The presence of IRD is not very common north of the 50°S in the CSP. The presence of IRD suggests the movement of large ice-bergs to the CSP and deposition of IRD took place during the period of warmer surface water due to the melting of large ice-bergs. Hence, this study has considered the abundance of IRD between 5.3 and 5.1 Ma, and between 4.9 and 4.5 Ma as the initiation of warm conditions at the CSP (Fig. 4b). The benthic foraminiferal species are suggesting variability between oxic and suboxic conditions at the CSP.

5.1.1. Dominant oxic benthic foraminifera ecology and interpreted conditions at CSP

Cibicidoides spp. can survive strong bottom currents and low flux of organic carbon (Linke and Lutze, 1993). Loubere and Fariduddin (1999) believed it indicated a significant seasonal food supply under oligotrophic settings. In the Indian Ocean, Cibicidoides spp. are associated with AABW (Corliss, 1979; Bremer and Lohmann, 1982), but in the Atlantic and Southern Ocean, they are associated with young, well-oxygenated water masses like NADW (Mackensen et al., 1995; Schmiedl and Mackensen, 1997; Gooday, 2003). Oridorsalis umbonatus is a cosmopolitan species capable of surviving in food-limited conditions. Most studies suggest that O. umbonatus prefers a well-oxygenated condition and low-organic carbon seafloor (Mackensen et al., 1995; Takata et al., 2019; Singh et al., 2021). Globocassidulina subglobosa is another cosmopolitan species that prefers well-oxygenated deep waters with

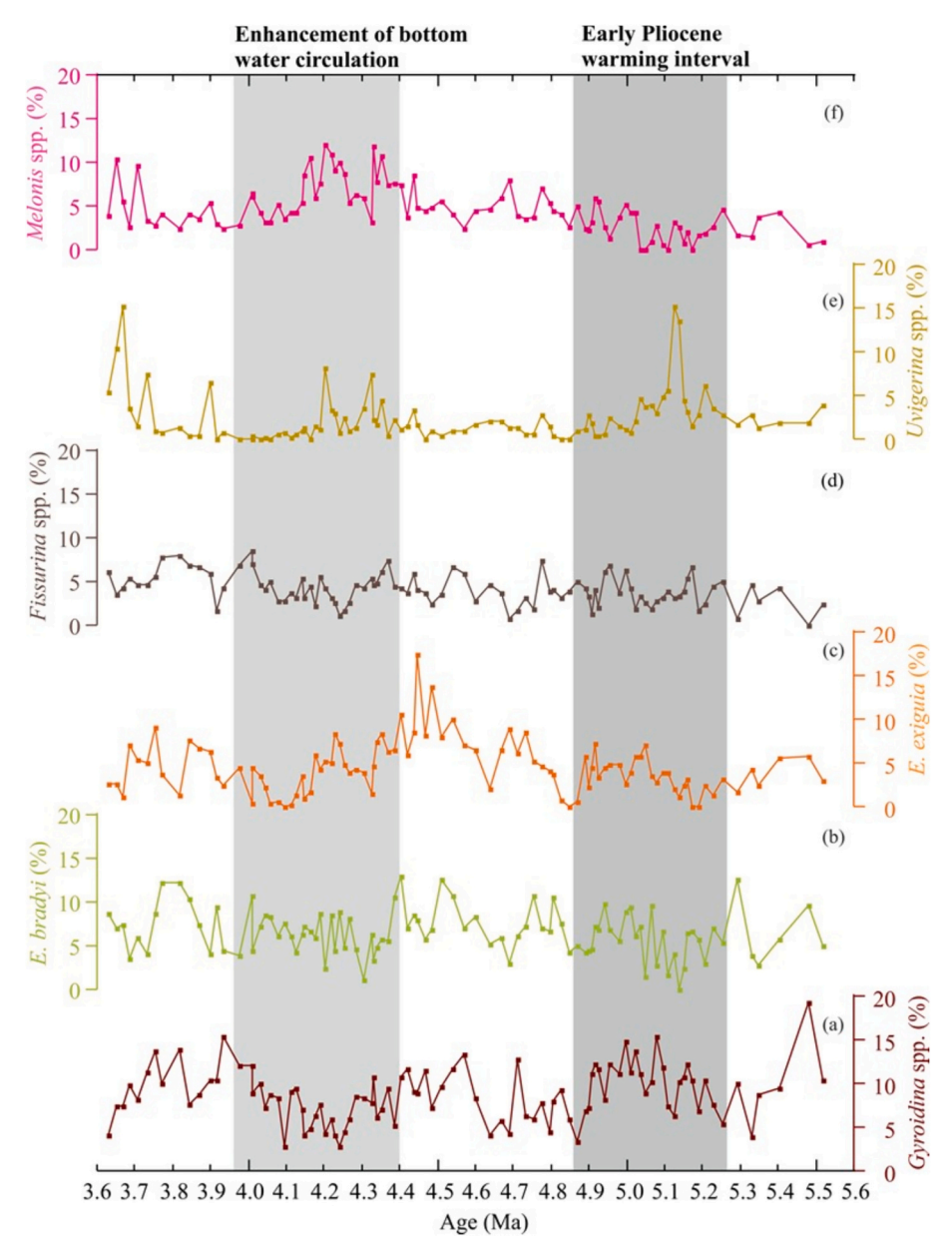


Fig. 6. Dominant suboxic benthic foraminifera assemblage (%) at Site U1541 plotted against interpolated ages, (a) *Gyroidina* spp. (%), (b) *Eggerella bradyi* (%), (c) *Epistominella exigua* (%), (d) *Fissurina* spp. (%), (e) *Uvigerina* spp. (%), (f) *Melonis* spp. (%), dark gray bar marks Early Pliocene warm interval, and light gray bar marks enhancement of bottom water circulation.

intermediate to strong food supply and is associated with the North Atlantic Deep Water (NADW) and AABW (Corliss, 1979; Das et al., 2021; Gupta et al., 2004; Singh et al., 2021). However, at CSP this species suggests higher productivity and better carbonate preservation and hence it also has a positive correlation with the suboxic assemblage along with *Pullenia* spp. (Fig. 8; Table 2).

Pullenia spp. encompasses shallow infaunal species associated with intermediate flux of organic matter in well-oxygenated deep waters of AABW origin (Bhaumik et al., 2007; Singh and Gupta, 2004; Verma et al., 2013). The occurrences of this species, have been linked to the occurrence of AABW (Bremer and Lohmann, 1982; Singh et al., 2012; Vats et al., 2021). It may withstand low organic carbon levels, strong bottom currents, and a strongly pulsed food supply (Linke and Lutze, 1993; Gupta, 1997). Laticarinina pauperata is an epifaunal species indicating deep southern source water like AABW (Gupta et al., 2006) and is found in cold, well-oxygenated deep waters in the Indian Ocean with a fluctuating flux of organic matter (Gupta and Thomas, 2003; Verma

et al., 2013). *L. pauperata* does not have any correlation with oxic species assemblages but the negative correlation with suboxic species assemblages and carbonate preservation suggests periods of enhanced AABW influence at the CSP. *Nuttallides umbonifera* exhibits a stronger relation with carbonate corrosivity and is found to be associated with cold, corrosive, oligotrophic, oxygenated deep water from the Pacific Ocean (Singh and Gupta, 2010; Singh et al., 2012). The species has been inferred to be an indicator of AABW (Mackensen et al., 1995; Singh and Gupta, 2004), whilst others have interpreted it as an indicator of low productivity and corrosive bottom water (Gooday, 1994; Loubere and Fariduddin, 1999; Singh et al., 2012, 2021).

The oxic species assemblage (Figs. 2, 5, 8, 9b) suggests well-oxygenated, strong bottom current conditions (LCDW with periodic strong pulses of AABW) with low to moderate organic carbon flux at CSP between 5.6 and 5.3 Ma, 4.9 and 4.6 Ma, and between 4.4 and 4.0 Ma (Fig. 9). The $\delta^{18}{\rm O}$ of *C. wuellerstorfi* in the South Atlantic has decreasing trend during 4.9–4.6 Ma and 4.3 and 4.0 Ma, which suggest an influence

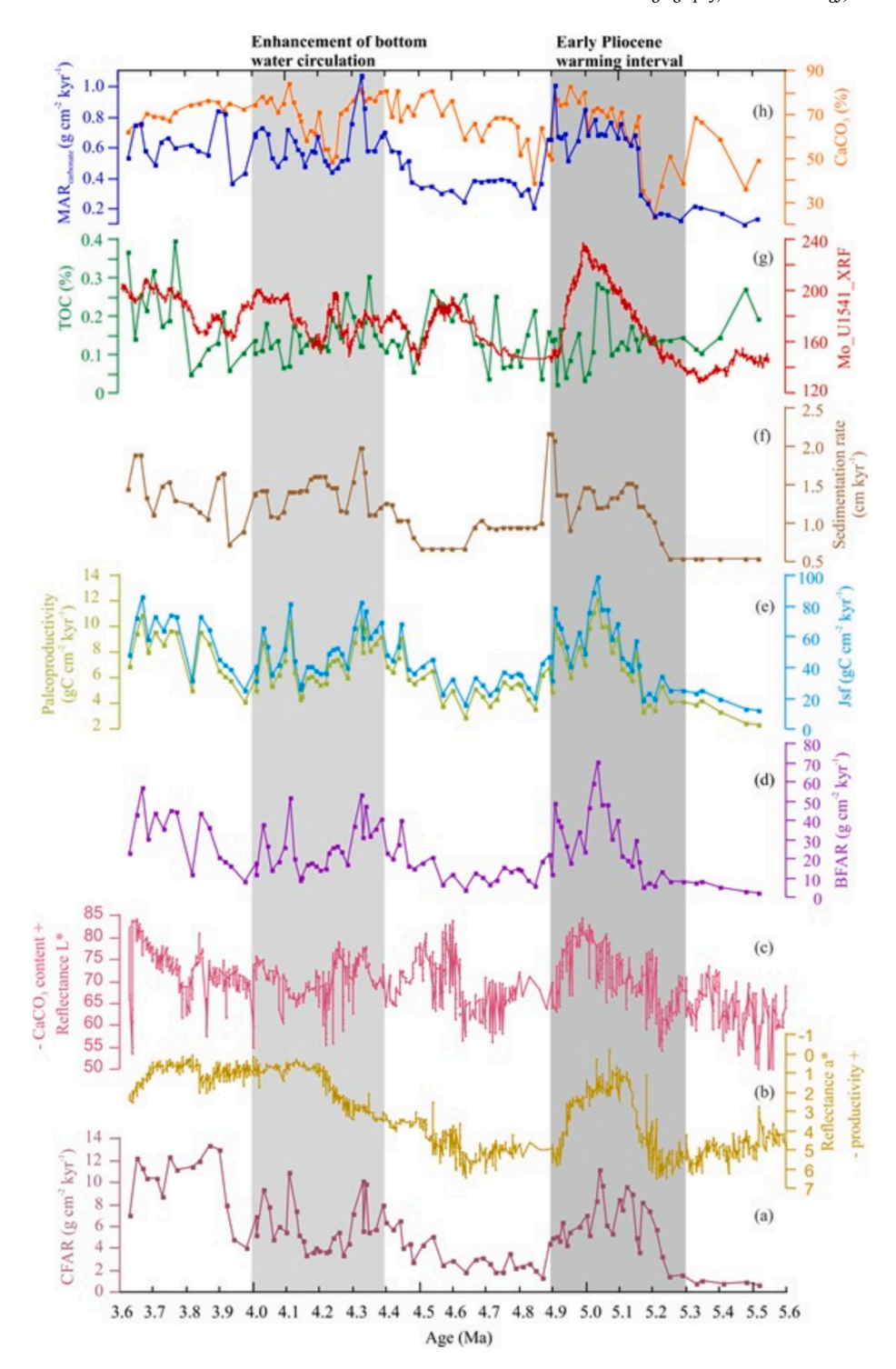


Fig. 7. The paleoproductivity parameters and carbonate preservation in the CSP plotted against interpolated ages. (a) Coarse Fraction Accumulation Rate (CFAR, g cm $^{-2}$ kyr $^{-1}$), (b) Color reflectance a* (Winckler et al., 2021), (c) Color reflectance L* (Winckler et al., 2021), (d) Benthic Foraminiferal Accumulation Rate (BFAR, g cm $^{-2}$ kyr $^{-1}$), (e) Sky blue curve: Organic flux to sea floor (J_{sf} , gC cm $^{-2}$ kyr $^{-1}$), and light green curve: Paleoproductivity (gC cm $^{-2}$ kyr $^{-1}$), (f) Sedimentation rate (cm kyr $^{-1}$), (g) Dark green curve: Total Organic Carbon (TOC, %), and red curve: Molybdenum (Mo, XRF data_U1541, Winckler et al., 2021), (h) Orange curve: Calcium carbonate (CaCO $_3$, %), and blue curve: CaCO $_3$ mass accumulation rate (MAR, g cm $^{-2}$ kyr $^{-1}$), dark gray bar marks Early Pliocene warm interval, and light gray bar marks enhancement of bottom water circulation. (For interpretation of the references to color in this figure legend, the reader is referred to the web version of this article.)

of stronger AABW (Fig. 9a; Karas et al., 2019).

5.1.2. Dominant suboxic benthic foraminifera ecology and interpreted conditions at CSP

Epifaunal to shallow infaunal microhabitat is preferred by Gyroidina

spp. (Rathburn and Corliss, 1994), while Gupta and Thomas (2003) found that the environment in which *Gyroidina* spp. thrived had an intermediate organic flux and intermediate to high seasonality. This species can be found in low-oxygen environments with variable food availability (De and Gupta, 2010). *Gyroidina* spp. can withstand low

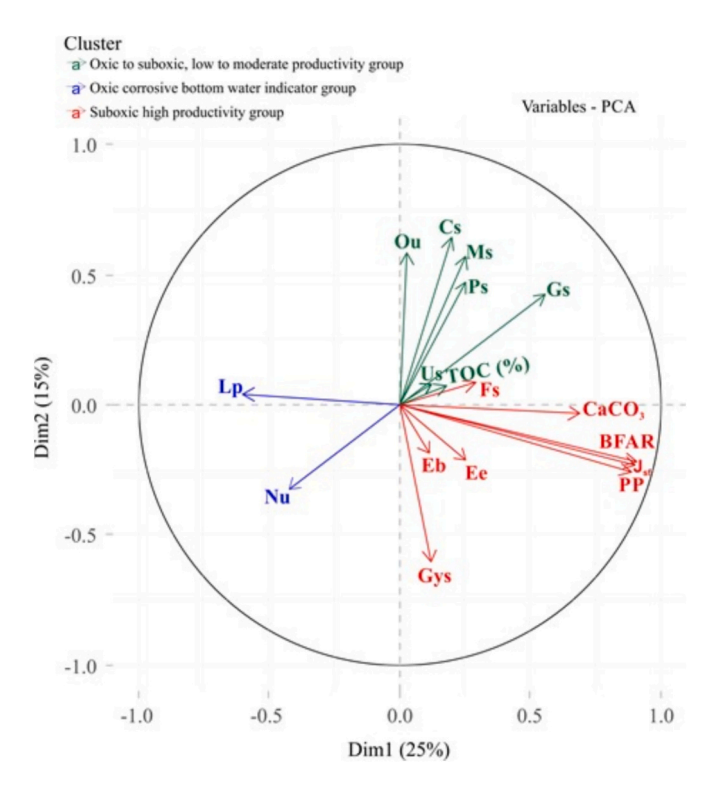


Fig. 8. Principal component analysis of the paleoproductivity parameters (Total Organic Carbon content (TOC, %), Benthic Foraminiferal Accumulation Rate (BFAR), Paleoproductivity (PP), and Organic flux to the seafloor (J_{sf}) , major species (Cs: Cibicidoides spp., Ou: Oridorsalis umbonatus, Lp: Laticarinina pauperata, Nu: Nuttallides umbonifera, Gs: Globocassidulina subglobosa, Gys: Gyroidina spp., Ms.: Melonis spp., Ee: Epistominella exigua, Ps: Pullenia spp., Eb: Eggerella bradyi, Us: Uvigerina spp., Fs: Fissurina spp.), and CaCO $_3$ (%) content.

oxygen conditions and shows a positive association with the productivity parameters in the CSP (Figs. 2, 6a). Eggerella bradyi environmental preference is not well constrained, however, it may indicate high organic flux with moderate degraded organic matter and low seasonality (Gupta et al., 2006; Bhaumik et al., 2007; De and Gupta, 2010). Epistominella exigua is a cosmopolitan species that exhibits opportunistic feeding behavior by consuming phytodetritus that is seasonally deposited on the sea floor (Gooday, 1993, 1994; Mackensen et al., 1995; Schmiedl et al., 1997; Das et al., 2021). E. exigua may be substantially more tolerant of low oxygen concentrations of 0.3 ml l⁻¹ (Jorissen et al., 2007; Erdem and Schönfeld, 2017). The higher abundance of this species is indicative of a higher input of phytodetritus to the sea floor and is linked to the suboxic high productivity group within the CSP (Fig. 6).

Fissurina spp. suggesting restricted phytodetritus input and indicative of low oxygen conditions (Mazumder and Nigam, 2014; Das et al., 2017) and its abundance suggest better carbonate preservation conditions at CSP (Figs. 6d, 8; Table 2). Uvigerina spp. are the shallow infaunal species, thrives in oxygen-depleted environments suggesting higher productivity with high sustained flux of organic matter (Figs. 6, 8; Table 2; Gupta et al., 2008; Gallagher et al., 2018; Das et al., 2018, 2021; Vats et al., 2021). Melonis is an infaunal genus found in suboxic environments, and frequently associated with degraded refractory organic matter (Schmiedl et al., 2000; Fontanier et al., 2002; Vats et al., 2021). This species has a positive correlation with the oxic to suboxic conditions with moderate flux of organic matter, suggesting its preferences for higher oxygenation conditions within the suboxic environment (Fig. 8; Table 2). This species abundance suggests higher productivity and better preservation conditions at CSP. These species association is abundant between 5.3 and 4.9 Ma, 4.6 and 4.4 Ma, and 4.0 and 3.6 Ma (Figs. 8, 9), suggesting seasonally enhanced flux of phytodetritus and degraded organic matter in suboxic conditions.

5.2. Paleoproductivity and organic carbon burial at the CSP

Several regional studies have shown that benthic foraminiferal population increase with carbon input to the sea floor (Herguera and Berger, 1991; Schmiedl and Mackensen, 1997; Diester-Haass and Faul, 2019). The flux of carbon from the ocean surface to the ocean floor determines the quantity of organic carbon (Corg) available for sequestration from the atmosphere-ocean system into sediments (Henson et al., 2012; Zhang et al., 2018). Surface water net primary productivity is the rate of C_{org} generation by photoautotrophs minus the rate of organic carbon loss (Henson et al., 2012) due to respiration. The total sedimentation rate controls the proportion of organic matter preservation and carbon burial in the marine sediment (Müller and Suess, 1979). The higher carbon burial rates are indicated by higher sedimentation rates and carbon flux to the seafloor. However, there are complexities in the vertical transport of organic matter from the ocean's surface to its depths, which changes not only with location but also in age (Boyd and Trull, 2007; Henson et al., 2012; Arndt et al., 2013). Since bacterial activity and grazing lead to remineralization of organic matter in the water column, biological pumping to sediments may be poor in regions with substantial vertical mixing despite high primary production and export productivity. Hence, PE_{eff} is high, and T_{eff} is low at high latitudes and the same is observed at the CSP (Fig. 3; Henson et al., 2012). While 30% of primary productivity is exported in the present Southern Ocean due to a high ratio of diatoms to total phytoplankton, only 5-10% of organic carbon exported from the photic zone survives to a depth of 2000 m (Henson et al., 2012) and this cause low TOC content at the studied site (Fig. 7g). In general, carbon burial rate is high when ocean productivity is high (Skinner et al., 2010). Molybdenum is another seawater redox proxy with a long residence time (Herrmann et al., 2012; Phillips and Xu, 2021) and its concentration well-matches with the TOC and BFAR records of Site U1541 (Fig. 7d, g), which further support periods of higher productivity in the CSP. However, BFAR shows a decreasing trend and low values during 4.7 to 4.5 Ma, which is inconsistent with the interpreted high productivity conditions as shown by the higher TOC (%). It might be due to the dominance of suboxic assemblages at the CSP, which is not reflected by the BFAR (Fig. 9; Naidu and Malmgren, 1995). The dominance of suboxic foraminiferal assemblage indicates a continuous and high food supply to the seafloor and oxygen deficiency during this interval (Fig. 9). These conditions were probably associated with a decrease in current strength, supported by the decrease in oxic assemblage and CFAR during this interval (Figs. 7a, 9). The foraminifera species G. subglobosa and Uvigerina spp. also show higher abundance during the period of high productivity (Figs. 5c, 6e) and are associated with productivity parameters (Figs. 7, 9). Thus, the combined higher productivity indicator proxies like Mo concentration, TOC content, BFAR, organic flux to the sea floor (Jsf), paleoproductivity estimation and sedimentation rate in the CSP suggest periods of higher productivity during the ~5.2-4.9 Ma, 4.6-4.3 Ma, 4.1 Ma, and 3.9-3.6 Ma (Figs. 7, 9).

5.3. Accumulation and preservation of carbonate

The lithofacies of the studied interval (from 85.2 to 105.9 m CCSF) mostly comprises of diatom-bearing calcareous/nannofossil ooze at Site U1541 (Winckler et al., 2021). CaCO₃ accumulation rates provide a measure of primary productivity originating from these calcareous primary producers (Diester-Haass et al., 2011) only if dissolution is negligible. The modern carbonate compensation depth (CCD) at CSP is located at ~4700 m water depth (Berger et al., 1976; Lyle, 2003), which is below the depths of the studied core (3604 m). Thus, we do not anticipate that foraminiferal carbonate was severely impacted by CCD. However, the presence of corrosive bottom water indicator species *N. umbonifera* (Mackensen et al., 1995; Smart et al., 2007; Singh and Gupta, 2010; Singh et al., 2021) in the sediment record reflects the influence of corrosive AABW at the studied site (Fig. 5h). The

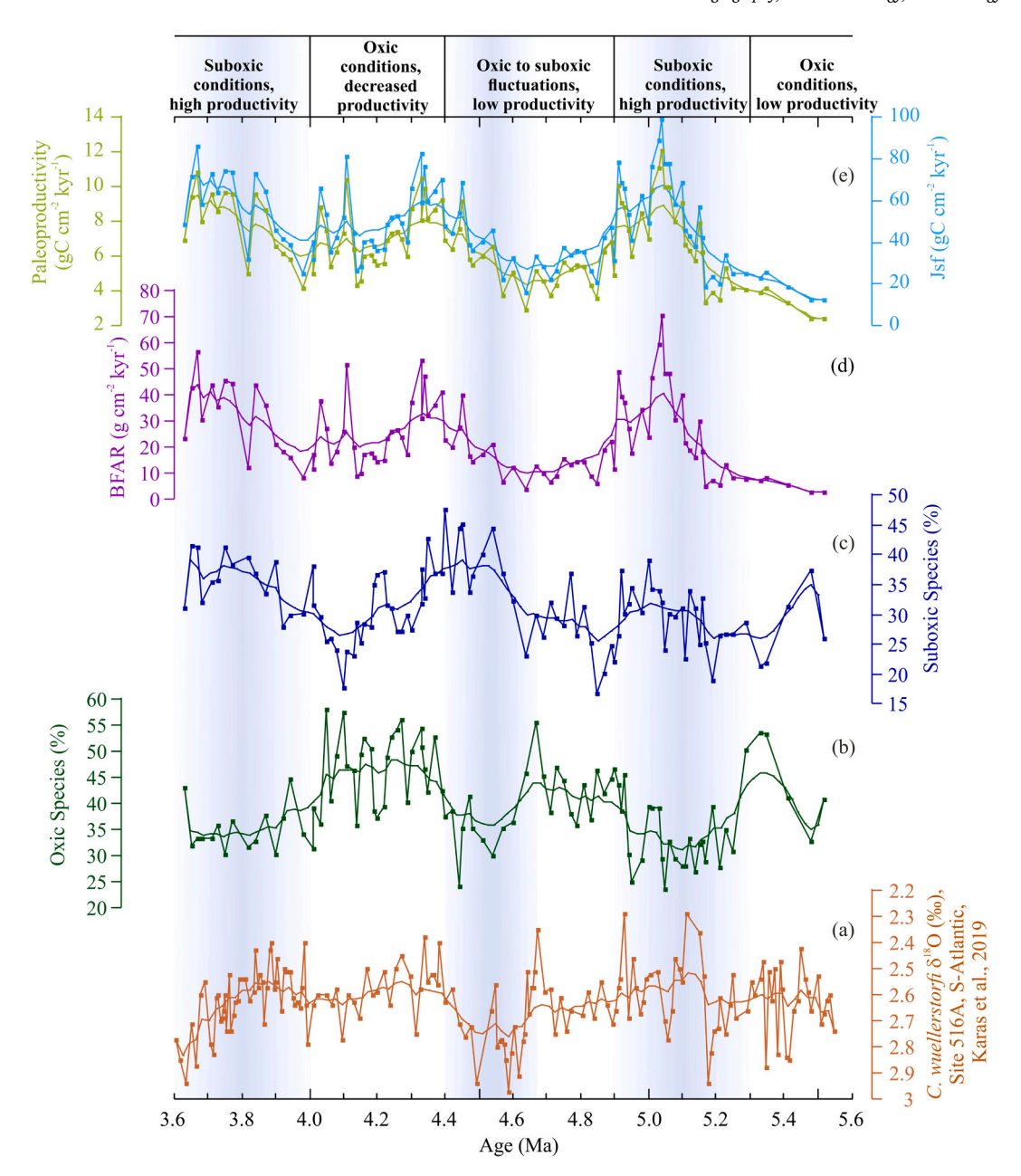


Fig. 9. Distribution of oxic and suboxic benthic foraminiferal assemblages with productivity parameters, (a) Cibicidoides wuellerstorfi (‰), Site 516 A, South Atlantic (Karas et al., 2019), (b) oxic species assemblage (%), (c) suboxic species assemblage (%), (d) Benthic Foraminiferal Accumulation Rate (BFAR, g cm⁻² kyr⁻¹), (e) Sky blue curve: Organic flux to sea floor (J_{sf} , gC cm⁻² kyr⁻¹), and light green curve: Paleoproductivity (gC cm⁻² kyr⁻¹). The color curves are smooth curve fit applied using KaleidaGraph software. The smooth curve fit function in KaleidaGraph software starts by applying a Stineman function to the data and the output has a geometric weight applied to the current point and \pm 10% of the data range. (For interpretation of the references to color in this figure legend, the reader is referred to the web version of this article.)

corrosiveness of the bottom waters (maximum in waters like AABW) may influence the distribution of the cosmopolitan taxa *N. umbonifera*, especially where strongly oligotrophic conditions prevail (Mackensen et al., 1995; Schmiedl et al., 1997). This species is found to be associated with *L. pauperata* and both have a negative correlation with the CaCO₃ (%) (Fig. 7; Table 2). However, the CFAR (g cm⁻² kyr⁻¹), color reflectance L*, MAR_{carbonate} (g cm⁻² kyr⁻¹), and CaCO₃ (%) suggest that the dissolution of calcium carbonate is not significant as reflected in our foraminifera data except for a period between 5.3 and 5.2 Ma, 4.9 and 4.6 Ma, and 4.3 and 4.2 Ma (Fig. 7). Higher abundance of *G. subglobosa*, *E. exigua*, and *Fissurina* spp. also suggests better carbonate preservation at CSP (Figs. 5, 6, 7; Table 2).

5.4. Paleoceanographic history of the Central South Pacific

The Late Miocene to Early Pliocene paleoceanographic evolution of the Central South Pacific is closely related to changes in the AABW and CDW circulation. The distribution of benthic foraminiferal species suggests significant changes in the LCDW circulation.

5.4.1. Late Messinian to Early Zanclean (5.6 to 4.9 Ma)

During the Late Messinian, CSP was well-ventilated and oxic in nature, marked by the presence of oxic species assemblage dominated by *Cibicidoides* spp., *O. umbonatus*, and *L. pauperata*. The bottom water was more corrosive marked by the occurrences of *N. umbonifera* and *L. pauperata* (Fig. 5e, f). The AABW influence was strongly marked by the

dominance of AABW indicator species like *Pullenia* spp., *Cibicidoides* spp., *O. umbonatus*, and *L. pauperata*. As indicated by the CFAR, L* value, MAR_{carbonate}, and CaCO₃ (%), carbonate preservation at CSP was extremely low between 5.6 and 5.3 Ma (Fig. 7). This is further supported by a negative correlation between CaCO₃ (%) and the corrosive bottom water indicator species (Fig. 8; Table 2). The Southern Ocean was moving towards warming conditions at ~5.3 Ma marked by the abundance of IRD (Fig. 4b) and planktic foraminifera *Orbulina universa* (Fig. 4c).

During the Early Zanclean period between 5.3 and 4.9 Ma, CSP was warmer compared to the pre-industrial revolution and highly productive at regular intervals, and had higher benthic foraminifera abundance (Fig. 4a). A rise in carbonate content was also observed during this period, as indicated by higher CFAR, L* value, CaCO₃ (%), and MAR-carbonate (Fig. 7). A significant increase in *Orbulina universa* (Fig. 4c) and decrease in 8¹⁸O of *C. wuellerstorfi* is observed in the South Atlantic, which also suggests warming during this interval (Fig. 9; Karas et al., 2019). The high productivity caused bottom water suboxic (Das et al., 2021), marked by the presence of *Uvigerina* spp., *Fissurina* spp., and other suboxic species (Fig. 6; Table 1). This period of high productivity is

contemporaneous with Late Miocene-Early Pliocene biogenic bloom inferred in all ocean basins (Dickens and Owen, 1999; Singh et al., 2012; Pillot et al., 2023). CDW production was sluggish during this period but had pulses of improved ventilation. Overall, this period was indicative of suboxic bottom water conditions with moderate to high organic flux, increased BFAR, and paleoproductivity (Figs. 9, 10a).

5.4.2. Early to Middle Zanclean (4.9 to 4.4 Ma)

Bottom water ventilation further improved between 4.9 and 4.6 Ma, marked by the presence of oxic species assemblage (Figs. 5, 9), decreasing trend of benthic foraminifera abundance per gram (Fig. 4a), maximum abundance of IRD (Fig. 4b), and declining trend in δ^{18} O of *C. wuellerstorfi* in the South Atlantic (Fig. 9; Karas et al., 2019). The BFAR, J_{sf}, paleoproductivity, TOC, CFAR, L* value, CaCO₃ (%), and MAR_{carbonate} were low during this interval. The overall bottom water current was strong and corrosive suggesting the influence of AABW marked by increasing abundance of *N. umbonifera* during 4.9 and 4.6 Ma (Fig. 5f). However, between 4.6 and 4.4 Ma, all the productivity proxies suggest higher productivity, increasing carbonate content and benthic foraminiferal assemblages suggest suboxic bottom water conditions

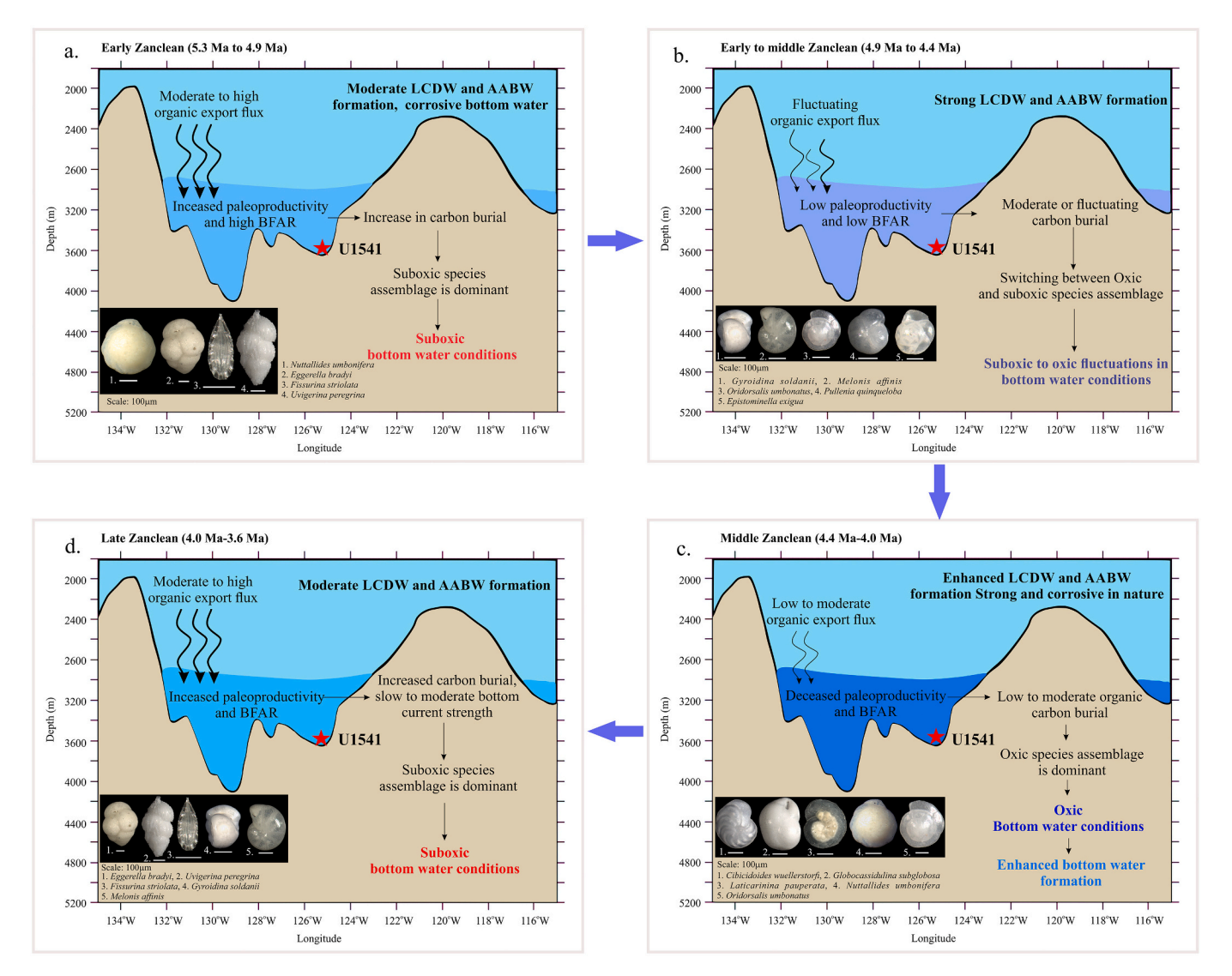


Fig. 10. Schematic illustration of paleoceanographic conditions at the CSP with photomicrographs of dominant species association during the periods given as (a) Early Zanclean (5.3–4.9 Ma), 1. Nuttallides umbonifera, 2. Eggerella bradyi, 3. Fissurina striolata, 4. Uvigerina peregrina, (b) Early to Middle Zanclean (4.9–4.4 Ma), 1. Gyroidina soldanii, 2. Melonis affinis, 3. Oridorsalis umbonatus, 4. Pullenia quinqueloba, 5. Epistominella exigua, (c) Middle Zanclean (4.4–4.0 Ma), 1. Cibicidoides wuellerstorfi, 2. Globocassidulina subglobosa, 3. Laticarinina pauperata, 4. Nuttallides umbonifera, 5. Oridorsalis umbonatus, (d) Middle to Late Zanclean (4.0–3.6 Ma), 1. Eggerella bradyi, 2. Uvigerina peregrina, 3. Fissurina striolata, 4. Gyroidina soldanii, 5. Melonis affinis.

(Figs. 7, 9). In general, this period was characterized by switch between oxic and suboxic bottom water conditions, modest to high organic flux, low BFAR, and paleoproductivity, with certain intermittent peak abundance (Figs. 9, 10b).

5.4.3. Middle Zanclean (4.4 to 4.0 Ma)

The CDW/AABW production was at its maximum between 4.4 and 4.0 Ma marked by oxic species assemblages (Figs. 5, 9). The CSP bottom water had low to moderate organic flux, well-oxygenated strong bottom water currents and dominance of CDW/AABW indicator species like *Pullenia* spp., *G. subglobosa, L. pauperata* and *Cibicidoides* spp. (Verma et al., 2013; Singh et al., 2012, 2021). Occasionally, bottom water was corrosive in nature marked by isolated peaks of *N. umbonifera*. The corrosive bottom water declines the CaCO₃ accumulation at CSP (Fig. 7). All the productivity proxies show declining trends during this interval, suggesting low productivity. In particular, this period had oxic bottom water conditions with a low to moderate organic flux, decreased BFAR, and low paleoproductivity (Figs. 9, 10c).

5.4.4. Late Zanclean (4.0 to 3.6 Ma)

The Southern Ocean was warm and more productive between 4.0 and 3.6 Ma marked by increased *Orbulina universa* abundances (Fig. 4c). Bottom water became suboxic, as indicated by the decreasing trend of oxic species and the increasing trend of suboxic species (Fig. 9). The CSP bottom water was overall suboxic during 4.0 to 3.6 Ma except for some transient moderate productivity events (Fig. 10d). Increases in a*, BFAR, TOC (%), CFAR, L* value, CaCO₃ (%), and MAR_{carbonate} suggest an increase in carbonate content and productivity over this period (Fig. 7). The bottom water production was moderate and kept influencing the subtropical Indian and Atlantic Oceans (Karas et al., 2019; Singh et al., 2021) marked by a significantly declining trend in δ^{18} O of *C. wuellerstorfi* in the South Atlantic (Fig. 9; Karas et al., 2019). A moderate to high organic flux, increased BFAR, high bottom water current strength, and higher paleoproductivity characterized this interval (Figs. 9, 10d).

5.5. Relation between paleoceanographic changes in the Southern Ocean and West Antarctic ice-sheet (WAIS) growth

During the Early Zanclean (5.3-4.9 Ma), conditions were generally warm throughout the world, and meridional temperature differences were quite modest (Pound et al., 2011; Herbert et al., 2016). The global gradual cooling trend was observed from ~4.4 Ma onwards due to the constriction of the Central American Seaway (CAS) and Indonesian throughflow. The closure of CAS strengthens the Atlantic Meridional Overturning Circulation (AMOC) and transports warm water towards the northern high latitude, which fosters the relatively cooling and strengthening of Southern Ocean deep water circulation (Karas et al., 2017, 2019). The benthic foraminiferal proxy suggests a stronger and more corrosive bottom water at CSP between 4.4 and 4.0 Ma (Figs. 5, 6, 7). The global overturning circulation, the Ross Sea gyre and the Weddell Sea gyre are primary sources of cold ocean bottom water (Fahrbach et al., 1995; Orsi et al., 1999, 2002; Orsi and Wiederwohl, 2009; Kerr et al., 2018). Supercooling and brine rejection of various water masses beneath floating ice shelves, particularly from the Ross Sea and the Weddell Sea, generates around 60-80% of LCDW and AABW (Nicholls et al., 2009; Orsi and Wiederwohl, 2009; Kerr et al., 2018). The northward migration of deep water from the source of LCDW and AABW has long been recognized as an important factor in ocean circulation and climate (Nowlin and Klinck, 1986; Duplessy et al., 1988). McKay et al. (2012) suggested that enhanced bottom and deep-water production intensifies the deep Southern Ocean ventilation. The significant increase in oxic species assemblage between 4.4 and 4.0 Ma suggests improved CSP ventilation due to stronger AABW and CDW influence (Fig. 5). The extension of the West Antarctic Ice Sheet (WAIS) from ~4.4 Ma onwards is supported by a stronger AABW formation, better Southern Ocean ventilation, and a colder deep ocean (Yin, 2013). The higher

oxygenation, lower bottom water temperature, and fluctuating carbonate dissolution rates in deep thermohaline circulation have been attributed to a major expansion of the Antarctic ice sheet and the related cooling in the Southern Ocean (Miller and Katz, 1987; Kurihara and Kennett, 1992; Yin, 2013), as well as a greatly diminished influx of warm saline deep water to the world ocean. Our data support enhanced deep water formation and deep ocean ventilation since 4.4 Ma, which may be linked with the strengthening of AMOC.

6. Conclusions

The distribution of benthic foraminifera at Site U1541 suggests that the organic matter flux and oxygenation in the CSP played an important controlling factor in productivity and deep-water circulation. During the Late Messinian to Early Zanclean (5.6 to 4.9 Ma), the deep CSP was wellventilated and oxic in nature, marked by the presence of oxic species assemblages, which slowly progressed towards suboxic environment at ~5.3 Ma due to increased productivity during the Early Pliocene warm interval. CSP was warmer and highly productive at regular intervals and had higher benthic foraminifera abundance. The Early Pliocene warming period in the CSP was characterized by higher abundances of IRD and Orbulina universa between 5.3 and 4.9 Ma. The CSP fluctuate between oxic and suboxic environment between 4.9 and 4.4 Ma with varied strength of bottom water. A rise in the proportion of oxic species assemblages in the CSP between 4.4 and 4.0 Ma suggests an enhancement in bottom water circulation (CDW or AABW), whose influence may have been observed in the subtropical Indian and Atlantic Oceans. The closure of the Central American Seaway may have triggered the same. The Southern Ocean again becomes warm and productive between 4.0 and 3.6 Ma.

CRediT authorship contribution statement

Sunil K. Das: Formal analysis, Data generation, Methodology, Writing - original draft, Writing - review & editing. N. Mahanta: Formal analysis, Writing – review & editing. B. Sahoo: Formal analysis, Writing - review & editing. Raj K. Singh: Conceptualization, Funding acquisition, Methodology, Supervision, Writing - original draft, Writing review & editing. Carlos A. Alvarez Zarikian: Formal analysis, Writing - review & editing, Data curation. Manish Tiwari: Formal analysis, Writing - review & editing. Nishant Vats: Formal analysis. Nihal: Formal analysis. Frank Lamy: Formal analysis, Data curation. Gisela Winckler: Formal analysis. Jennifer L. Middleton: Data curation. Helge W. Arz: Data curation. Julia Gottschalk: Data curation. Chandranath Basak: Data curation. Anieke Brombacher: Data curation. Oliver M. Esper: Data curation. Jesse R. Farmer: Data curation. Lisa C. Herbert: Data curation. Shinya Iwasaki: Data curation. Lester Lembke-Jene: Data curation. Vera J. Lawson: Data curation. Li Lo: Data curation. Elisa Malinverno: Data curation. Elisabeth Michel: Data curation. Simone Moretti: Data curation. Christopher M. Moy: Data curation. Ana Christina Ravelo: Data curation. Christina R. Riesselman: Data curation. Mariem Saavedra-Pellitero: Data curation. Inah Seo: Data curation. Rebecca A. Smith: Data curation. Alexandre L. Souza: Data curation. Joseph S. Stoner: Data curation. Igor Venancio M.P. de Oliveira: Data curation. Sui Wan: Data curation. Xiangyu Zhao: Data curation.

Declaration of competing interest

The authors declare no competing financial interests.

Data availability

Data on the major benthic foraminiferal percentage abundance from Site U1541 were generated for this study covering Late Miocene to Early Pliocene epoch. Data regarding dominant benthic foraminiferal abundance (%, present in >7% in 7 or more sample), oxic species assemblage (%), suboxic species assemblage (%), sedimentation rate (cm kyr $^{-1}$), Dry Bulk Density (g cm $^{-3}$), *Orbulina universa* (>125 µm), Ostracoda (>125 µm), ice-rafted debris (IRD) & detrital (>125 µm), and benthic foraminifera (>125 µm) per gram of dry sediment, and benthic foraminiferal accumulation rate (BFAR, g cm $^{-2}$ kyr $^{-1}$), organic flux (Jsf, gC cm $^{-2}$ kyr $^{-1}$), paleoproductivity (PP, gC cm $^{-2}$ kyr $^{-1}$), total organic carbon (%), CaCO $_3$ (%), coarse fraction (%, >63 µm), and Coarse Fraction Accumulation Rate (CFAR, g cm $^{-2}$ kyr $^{-1}$) are available in Mendeley data, doi:10.17632/dfbrc8dtrm.2.

Acknowledgments

The International Ocean Discovery Program is thankfully acknowledged for providing core samples to RKS. RKS, MT and SKD acknowledge the financial support given by the ESSO-National Centre for Polar and Ocean Research, Ministry of Earth Sciences, under the IODP initiative to undertake this research (RP-277). SKD and NM acknowledges DST for the INSPIRE Fellowship (IF180859 and IF190584 respectively) and IIT Bhubaneswar for the infrastructure facility. RKS acknowledge SERB (CRG/2020/000396) for support. CAZ acknowledges financial support from the US National Science Foundation, award OCE-1326927. MT thanks the Secretary, Ministry of Earth Sciences (MoES) and Director, ESSO-National Centre for Polar and Ocean Research (NCPOR Contribution no. J-2/2024-25) for support.

References

- Alvarez Zarikian, C.A., 2015. Cenozoic bathyal and abyssal ostracods beneath the oligotrophic south pacific gyre (IODP expedition 329 sites U1367, U1368 and U1370). Palaeogeogr. Palaeoclimatol. Palaeoecol. 419 (1), 115–142. https://doi. org/10.1016/j.palaeo.2014.07.024.
- Arndt, S., Jørgensen, B.B., LaRowe, D.E., Middelburg, J.J., Pancost, R.D., Regnier, P., 2013. Quantifying the degradation of organic matter in marine sediments: a review and synthesis. Earth-Sci. Rev. 123, 53–86. https://doi.org/10.1016/j. earscirev.2013.02.008.
- Balsam, W.L., Deaton, B.C., Damuth, J.E., 1999. Evaluating optical lightness as a proxy for carbonate content in marine sediment cores. Mar. Geol. 161 (2-4), 141–153. https://doi.org/10.1016/S0025-3227(99)00037-7.
- Barker, P.F., Burrell, J., 1977. The opening of Drake passage. Mar. Geol. 25 (1–3), 15–34. https://doi.org/10.1016/0025-3227(77)90045-7.
- Berger, W.H., Adelseck, C.G., Mayer, L.A., 1976. Distribution of carbonate in surface sediments of the Pacific Ocean. J. Geophys. Res. 81 (15), 2617–2627. https://doi. org/10.1029/jc081i015p02617.
- Bhaumik, A.K., Gupta, A.K., Sundar Raj, M., Mohan, K., De, S., Sarkar, S., 2007.
 Paleoceanographic evolution of the northeastern Indian ocean during the Miocene: evidence from deep-sea benthic foraminifera (DSDP Hole 216A). Indian J. Mar. Sci. 36 (4), 332–341. http://nopr.niscpr.res.in/handle/123456789/57.
- Billmeyer, F.W., Saltzman, M., 1981. Principles of Color Technology, 2nd ed. Wiley, New York.
- Boyd, P.W., Trull, T.W., 2007. Understanding the export of biogenic particles in oceanic waters: is there consensus? Prog. Oceanogr. 72 (4), 276–312. https://doi.org/ 10.1016/j.pocean.2006.10.007.
- Bremer, M.L., Lohmann, G.P., 1982. Evidence for primary control of the distribution of certain Atlantic Ocean benthonic foraminifera by degree of carbonate saturation. Deep Sea Res. A Oceanogr. Res. Pap. 29 (8), 987–998. https://doi.org/10.1016/ 0198-0149(82)90022-X.
- Carter, L., McCave, I.N., Williams, M.J.M., 2008. Chapter 4 circulation and water masses of the Southern Ocean: a review. Dev. Earth Environ. Sci. 8 (8), 85–114. https://doi. org/10.1016/S1571-9197(08)00004-9.
- Carter, L., Bostock-Lyman, H., Bowen, M., 2022. Water masses, circulation and change in the modern Southern Ocean. In: Antarctic Climate Evolution, pp. 165–197. https:// doi.org/10.1016/B978-0-12-819109-5.00003-7.
- Corliss, B.H., 1979. Recent deep-sea benthonic foraminiferal distributions in the Southeast Indian Ocean: inferred bottom-water routes and ecological implications. Mar. Geol. 31 (1–2), 115–138. https://doi.org/10.1016/0025-3227(79)90059-8.
- Das, M., Singh, R.K., Gupta, A.K., Bhaumik, A.K., 2017. Holocene strengthening of the oxygen minimum zone in the northwestern Arabian Sea linked to changes in intermediate water circulation or Indian monsoon intensity? Palaeogeogr. Palaeoclimatol. Palaeoecol. 483, 125–135. https://doi.org/10.1016/j. palaeo.2016.10.035.
- Das, M., Singh, R.K., Vats, N., Holbourn, A., Mishra, S., Farooq, S.H., Pandey, D.K., 2018. Changes in the distribution of Uvigerinidae species over the past 775 kyr: implications for the paleoceanographic evolution of the Japan Sea. Palaeogeogr. Palaeoclimatol. Palaeoecol. 507, 201–213. https://doi.org/10.1016/j. palaeo.2018.07.019.

- Das, M., Singh, R.K., Holbourn, A., Farooq, S.H., Vats, N., Pandey, D.K., 2021.
 Paleoceanographic evolution of the Japan Sea during the Pleistocene a benthic foraminiferal perspective. Palaeogeogr. Palaeoclimatol. Palaeoecol. 566, 110238 https://doi.org/10.1016/j.palaeo.2021.110238.
- de Araújo, H.A.B., Dominguez, J.M.L., de Machado, A.J., de Rangel, A.G.A.N., 2018. Benthic foraminifera distribution in a deltaic clinoform (São Francisco Delta, eastern Brazil): a reference study. J. Mar. Syst. 186, 1–16. https://doi.org/10.1016/j.jmarsys.2018.05.004.
- De, S., Gupta, A.K., 2010. Deep-sea faunal provinces and their inferred environments in the Indian Ocean based on distribution of recent benthic foraminifera. Palaeogeogr. Palaeoclimatol. Palaeoecol. 291 (3–4), 429–442. https://doi.org/10.1016/j. palaeo. 2010.03.012
- Dickens, G.R., Owen, R.M., 1999. The latest Miocene–Early Pliocene biogenic bloom: a revised Indian Ocean perspective. Mar. Geol. 161 (1), 75–91. https://doi.org/ 10.1016/S0025-3227(99)00057-2
- Diester-Haass, L., 1995. Middle eocene to early oligocene paleoceanography of the Antarctic Ocean (Maud rise, ODP Leg 113, Site 689): change from a low to a high productivity ocean. Palaeogeogr. Palaeoclimatol. Palaeoecol. 113 (2–4), 311–334. https://doi.org/10.1016/0031-0182(95)00067-v.
- Diester-Haass, L., Faul, K., 2019. Paleoproductivity reconstructions for the Paleogene Southern Ocean: a direct comparison of geochemical and micropaleontological proxies. Paleoceanogr. Paleoclimatol. 34 (1), 79–97. https://doi.org/10.1029/ 2018PA003384.
- Diester-Haass, L., Billups, K., Emeis, K., 2011. Enhanced paleoproductivity across the Oligocene/Miocene boundary as evidenced by benthic foraminiferal accumulation rates. Palaeogeogr. Palaeoclimatol. Palaeoecol. 302 (3–4), 464–473. https://doi.org/10.1016/j.palaeo.2011.02.006.
- Duplessy, J.C., Shackleton, N.J., Fairbanks, R.G., Labeyriefi, L., Oppo, D., Kallel, N., 1988. Deepwater source variations during the last climatic cycle and their impact on the global deepwater circulation. Paleoceanography 3 (3), 343–360. https://doi.org/ 10.1029/PA003i003p00343.
- Erdem, Z., Schönfeld, J., 2017. Pleistocene to Holocene benthic foraminiferal assemblages from the Peruvian continental margin. Palaeontol. Electron. 20 (2). Art-Nr.
- Erdem, Z., Schönfeld, J., Rathburn, A.E., Pérez, M.E., Cardich, J., Glock, N., 2020. Bottom-water deoxygenation at the Peruvian margin during the last deglaciation recorded by benthic foraminifera. Biogeosciences 17 (12), 3165–3182. https://doi. org/10.5194/bg-17-3165-2020.
- Fahrbach, E., Rohardt, G., Scheele, N., Schroder, M., Strass, V., Wisotzki, A., 1995.
 Formation and discharge of deep and bottom water in the northwestern Weddell Sea.
 J. Mar. Res. 53 (4), 515–538. https://doi.org/10.1357/0022240953213089.
- Fontanier, C., Jorissen, F.J., Licari, L., Alexandre, A., Anschutz, P., Carbonel, P., 2002. Live benthic foraminiferal faunas from the Bay of Biscay: faunal density, composition, and microhabitats. Deep Sea Res. I Oceanogr. Res. Pap. 49 (4), 751–785. https://doi.org/10.1016/S0967-0637(01)00078-4.
- Gallagher, S.J., Sagawa, T., Henderson, A.C.G., Saavedra-Pellitero, M., De Vleeschouwer, D., Black, H., Itaki, T., Toucanne, S., Bassetti, M.A., Clemens, S., Anderson, W., Alvarez-Zarikian, C., Tada, R., 2018. East Asian monsoon history and paleoceanography of the Japan Sea over the last 460,000 years. Paleoceanogr. Paleoclimatol. 33 (7), 683–702. https://doi.org/10.1029/2018PA003331.
- Garcia, H.E., Locarnini, R.A., Boyer, T.P., Antonov, J.I., Baranova, O.K., Zweng, M.M., Reagan, J.R., Johnson, D.R., 2013. World Ocean Atlas 2013. Vol. 4: dissolved inorganic nutrients (phosphate, nitrate, silicate). In: Levitus, S. (Ed.), A. Mishonov, Technical Ed. NOAA Atlas NESDIS, 76, p. 25 dataset. https://doi.org/10.7289/ //SE76GCT
- Gastaldello, M.E., Agnini, C., Westerhold, T., Drury, A.J., Sutherland, R., 2023. The Late Miocene-Early Pliocene biogenic bloom: an integrated study in the Tasman Sea. Paleoceanogr. Paleoclimatol. https://doi.org/10.1029/2022PA004565.
- Gille-Petzoldt, J., Gohl, K., Uenzelmann-Neben, G., Grützner, J., Klages, J.P., IODP Expedition 379 Scientists, 2022. West Antarctic ice sheet dynamics in the Amundsen Sea sector since the Late Miocene—tying IODP expedition 379 results to seismic data. Front. Earth Sci. 10 https://doi.org/10.3389/feart.2022.976703.
- Giosan, L., Flood, R.D., Aller, R.C., 2002. Paleoceanographic significance of sediment color on western North Atlantic drifts: I. Origin of color. Mar. Geol. 189, 25–41. https://doi.org/10.1016/S0025-3227(02)00321-3.
- Gohl, K., Uenzelmann-Neben, G., Gille-Petzoldt, J., Hillenbrand, C.D., Klages, J.P., Bohaty, S.M., IODP Expedition 379 Scientists, 2021. Evidence for a highly dynamic West Antarctic ice sheet during the Pliocene. Geophys. Res. Lett. 48 (14) https://doi. org/10.1029/2021GL093103.
- Gooday, A.J., 1993. Deep-sea benthic foraminiferal species which exploit phytodetritus: characteristic features and controls on distribution. Mar. Micropaleontol. 22 (3), 187–205. https://doi.org/10.1016/0377-8398(93)90043-W.
- Gooday, A.J., 1994. The biology of deep-sea foraminifera: a review of some advances and their applications in paleoceanography. Palaios 14–31. https://doi.org/10.2307/ 3515075
- Gooday, A.J., 2003. Benthic foraminifera (protista) as tools in deep-water palaeoceanography: environmental influences on faunal characteristics. Adv. Mar. Biol. 46, 1–90. https://doi.org/10.1016/S0065-2881(03)46002-1.
- Gupta, A.K., 1997. Paleoceanographic and paleoclimatic history of the Somali Basin during the Pliocene-Pleistocene: multivariate analyses of benthic foraminifera from DSDP site 241 (leg 25). J. Foraminifer. Res. 27 (3), 196–208. https://doi.org/ 10.2113/gsifr.27.3.196.
- Gupta, A.K., Thomas, E., 2003. Initiation of Northern Hemisphere glaciation and strengthening of the northeast Indian monsoon: ocean drilling program site 758, eastern equatorial Indian Ocean. Geology 31 (1), 47–50. https://doi.org/10.1130/ 0091-7613(2003)031<0047:IONHGA>2.0.CO;2.

- Gupta, A.K., Singh, R.K., Joseph, S., Thomas, E., 2004. Indian Ocean high-productivity event (10-8 Ma): linked to global cooling or to the initiation of the Indian monsoons? Geology 32 (9), 753–756. https://doi.org/10.1130/G20662.1.
- Gupta, A.K., Das, M., Bhaskar, K., 2006. South equatorial current (SEC) driven changes at DSDP site 237, Central Indian Ocean, during the Plio-Pleistocene: evidence from benthic foraminifera and stable isotopes. J. Asian Earth Sci. 28 (4–6), 276–290. https://doi.org/10.1016/i.jseaes.2005.10.006.
- Gupta, A.K., Das, M., Clemens, S.C., Mukherjee, B., 2008. Benthic foraminiferal faunal and isotopic changes as recorded in Holocene sediments of the Northwest Indian Ocean. Paleoceanography 23 (2). https://doi.org/10.1029/2007PA001546.
- Hemleben, C., Spindler, M., Anderson, O.R., 1989. Taxonomy and species features. In: Modern Planktonic Foraminifera, 1897, pp. 8–32. https://doi.org/10.1007/978-1-4612-3544-6.2
- Henson, S.A., Sanders, R., Madsen, E., 2012. Global patterns in efficiency of particulate organic carbon export and transfer to the deep ocean. Glob. Biogeochem. Cycles 26 (1), 1–14. https://doi.org/10.1029/2011GB004099.
- Herbert, T.D., Lawrence, K.T., Tzanova, A., Peterson, L.C., Caballero-Gill, R., Kelly, C.S., 2016. Late Miocene global cooling and the rise of modern ecosystems. Nat. Geosci. 9 (11), 843–847. https://doi.org/10.1038/NGEO2813.
- Herguera, J.C., 2000. Last glacial paleoproductivity patterns in the eastern equatorial Pacific: benthic foraminifera records. Mar. Micropaleontol. 40 (3), 259–275. https://doi.org/10.1016/S0377-8398(00)00041-4.
- Herguera, J.C., Berger, W.H., 1991. Paleoproductivity from benthic foraminifera abundance: glacial to postglacial change in the West-Equatorial Pacific. Geology 19 (12), 1173–1176. https://doi.org/10.1130/0091-7613(1991)019<1173: PFBFAG>2.3.CO;2.
- Herraiz-Borreguero, L., Rintoul, S.R., 2011. Subantarctic mode water: distribution and circulation. Ocean Dyn. 61 (1), 103–126. https://doi.org/10.1007/s10236-010-0352-9
- Herrmann, A.D., Kendall, B., Algeo, T.J., Gordon, G.W., Wasylenki, L.E., Anbar, A.D., 2012. Anomalous molybdenum isotope trends in Upper Pennsylvanian euxinic facies: significance for use of 898Mo as a global marine redox proxy. Chem. Geol. 324, 87–98. https://doi.org/10.1016/j.chemgeo.2012.05.013.
- Holbourn, A., Kuhnt, W., Frank, M., Haley, B.A., 2013. Changes in Pacific Ocean circulation following the Miocene onset of permanent Antarctic ice cover. Earth Planet. Sci. Lett. 365, 38–50. https://doi.org/10.1016/j.epsl.2013.01.020.
- Jiang, H., Yu, L., Xu, H., Vetter, P.A., 2020. Evaluation of global ocean models on simulating the deep western boundary current in the Pacific. Atmosphere-Ocean 58 (3), 219–230. https://doi.org/10.1080/07055900.2020.1789547.
- Jorissen, F.J., de Stigter, H.C., Widmark, J.G.V., 1995. A conceptual model explaining benthic foraminiferal microhabitats. Mar. Micropaleontol. 26 (1–4), 3–15. https:// doi.org/10.1016/0377-8398(95)00047-X.
- Jorissen, F.J., Fontanier, C., Thomas, E., 2007. Chapter seven paleoceanographical proxies based on deep-sea benthic foraminiferal assemblage characteristics. Dev. Mar. Geol. 1, 263–325. https://doi.org/10.1016/S1572-5480(07)01012-3.
- Kaiho, K., 1994. Benthic foraminiferal dissolved-oxygen index and dissolved-oxygen levels in the modern ocean. Geology 22 (8), 719–722. https://doi.org/10.1130/0091-7613(1994)022</719-BEDOIA > 2.3 CO:2
- Kaithwar, A., Singh, D.P., Saraswat, R., 2020. A highly diverse living benthic foraminiferal assemblage in the oxygen deficient zone of the southeastern Arabian Sea. Biodivers. Conserv. 29, 3925–3958. https://doi.org/10.1007/s10531-020-02056.
- Karas, C., Nürnberg, D., Tiedemann, R., Garbe-Schönberg, D., 2011. Pliocene climate change of the Southwest Pacific and the impact of ocean gateways. Earth Planet. Sci. Lett. 301 (1–2), 117–124. https://doi.org/10.1016/j.epsl.2010.10.028.
- Karas, C., Nürnberg, D., Bahr, A., Groeneveld, J., Herrle, J.O., Tiedemann, R., Demenocal, P.B., 2017. Pliocene oceanic seaways and global climate. Sci. Rep. 7 https://doi.org/10.1038/srep39842.
- Karas, C., Goldstein, S.L., deMenocal, P.B., 2019. Evolution of Antarctic intermediate water during the Plio-Pleistocene and implications for global climate: evidence from the South Atlantic. Quat. Sci. Rev. 223 https://doi.org/10.1016/j. guascirev.2019.105945.
- Kawabe, M., Fujio, S., 2010. Pacific Ocean circulation based on observation. J. Oceanogr. 66 (3), 389–403. https://doi.org/10.1007/s10872-010-0034-8.
- Kennett, J.P., 1977. Cenozoic evolution of Antarctic glaciation, the circum-Antarctic Ocean, and their impact on global paleoceanography. J. Geophys. Res. 82 (27), 3843–3860. https://doi.org/10.1029/jc082i027p03843.
- Kerr, R., Dotto, T.S., Mata, M.M., Hellmer, H.H., 2018. Three decades of deep water mass investigation in the Weddell Sea (1984–2014): temporal variability and changes. Deep-Sea Res. II Top. Stud. Oceanogr. 149, 70–83. https://doi.org/10.1016/j. dsr2.2017.12.002.
- Kuhlbrodt, T., Griesel, A., Montoya, M., Levermann, A., Hofmann, M., Rahmstorf, S., 2007. On the driving processes of the Atlantic meridional overturning circulation. Rev. Geophys. 45 (2) https://doi.org/10.1029/2004RG000166.
- Kurihara, K., Kennett, J.P., 1992. Paleoceanographic significance of Neogene benthic foraminiferal changes in a Southwest Pacific bathyal depth transect. Mar. Micropaleontol. 19 (3), 181–199. https://doi.org/10.1016/0377-8398(92)90028-I.
- Lamy, F., Winckler, G., Alvarez Zarikian, C.A., Arz, H.W., Basak, C., Brombacher, A., Esper, O.M., Farmer, J.R., Gottschalk, J., Herbert, L.C., Iwasaki, S., Lawson, V.J., Lembke-Jene, L., Lo, L., de Souza, A.L., Malinverno, E., Michel, E.M.L., Middleton, J., Moretti, S., Wilkins, A., 2019. Expedition 383 preliminary report dynamics of the Pacific Antarctic Circumpolar Current (DYNAPACC). Int. Ocean Discov. Progr. Prelim. Rep. 383, 1–81. https://doi.org/10.14379/iodp.pr.383.2019.
- Lamy, F., Winckler, G., Arz, H.W., Farmer, J.R., Gottschalk, J., Lembke-Jene, L., Middleton, J.L., van der Does, M., Tiedemann, R., Zarikian, C.A., Basak, C., Brombacher, A., Dumm, L., Esper, O.M., Herbert, L.C., Iwasaki, S., Kreps, G.,

- Lawson, V.J., Lo, L., Malinverno, E., Martinez-Garcia, A., Michel, E., Moretti, S., Moy, C.M., Ravelo, A.C., Riesselman, C.R., Saavedra-Pellitero, M., Sadatzki, H., Seo, I., Singh, R.K., Smith, R.A., Souza, A.L., Stoner, J.S., Toos, M., de Oliveira, I.M. V.P., Wan, S., Wu, S., Zhao, X., 2024. Five million years of Antarctic Circumpolar Current strength variability. Nature 627 (8005). https://doi.org/10.1038/s41586-024-07143-3
- Lê, S., Josse, J., Husson, F., 2008. FactoMineR: an R package for multivariate analysis. J. Stat. Softw. 25 (1), 253–258. https://doi.org/10.18637/jss.v025.i01.
- Linke, P., Lutze, G.F., 1993. Microhabitat preferences of benthic foraminifera a static concept or a dynamic adaptation to optimize food acquisition? Mar. Micropaleontol. 20 (3–4), 215–234. https://doi.org/10.1016/0377-8398(93)90034-U.
- Liu, Z., Tuo, S., Zhao, Q., Cheng, X., Huang, W., 2004. Deep-water earliest Oligocene glacial maximum (EOGM) in South Atlantic. Chin. Sci. Bull. 49, 2190–2197. https:// doi.org/10.1007/BF03185787.
- Loeblich, A.R., Tappan, H., 1988. Foraminiferal Genera and their Classification, p. 970.
 Loubere, P., Fariduddin, M., 1999. Benthic foraminifera and the flux of organic carbon to the seabed. In: Sengupta, B. (Ed.), Modern Foraminifera, pp. 181–199. https://doi.org/10.1007/0-306-48104-9 11.
- Lübbers, J., Kuhnt, W., Holbourn, A.E., Bolton, C.T., Gray, E., Usui, Y., Andersen, N., 2019. The middle to late Miocene "carbonate crash" in the equatorial Indian Ocean. Paleoceanogr. Paleoclimatol. 34 (5), 813–832. https://doi.org/10.1029/ 2018PA003482.
- Lyle, M., 2003. Neogene carbonate burial in the Pacific Ocean. Paleoceanography 18 (3), 1–19. https://doi.org/10.1029/2002pa000777.
- Mackensen, A., 2004. Changing Southern Ocean palaeocirculation and effects on global climate. Antarct. Sci. 16 (4), 369–386. https://doi.org/10.1017/ S0954102004002202.
- Mackensen, A., Schmiedl, G., Harloff, J., Giese, M., 1995. Deep-sea foraminifera in the South Atlantic Ocean: ecology and assemblage generation. Micropaleontology 41 (4), 342–358. https://doi.org/10.2307/1485808.
- Majoran, S., Dingle, R.V., 2002. Cenozoic deep-sea ostracods from Maud rise, Weddell Sea, Antarctica (ODP Site 689): a palaeoceanographical perspective. Geobios 35 (1), 137–152. https://doi.org/10.1016/S0016-6995(02)00016-5.
- Marshall, J., Speer, K., 2012. Closure of the meridional overturning circulation through Southern Ocean upwelling. Nat. Geosci. 5 (3), 171–180. https://doi.org/10.1038/
- Mazumder, A., Nigam, R., 2014. Bathymetric preference of four major genera of rectilinear benthic foraminifera within oxygen minimum zone in Arabian Sea off central west coast of India. J. Earth Syst. Sci. 123 (3), 633–639. https://doi.org/ 10.1007/s12040-014-0419-y.
- McKay, R., Naish, T., Carter, L., Riesselman, C., Dunbar, R., Sjunneskog, C., Winter, D., Sangiorgi, F., Warren, C., Pagani, M., Schouten, S., Willmott, V., Levy, R., DeConto, R., Powell, R.D., 2012. Antarctic and Southern Ocean influences on Late Pliocene global cooling. Proc. Natl. Acad. Sci. USA 109 (17), 6423–6428. https://doi.org/10.1073/pnas.1112248109.
- Miller, K.G., Katz, M.E., 1987. Eocene benthic foraminiferal biofacies of the New Jersey transect. In: Initial Reports DSDP, Leg, 95, pp. 267–298. https://doi.org/10.2973/ dsdp.proc.95.107.1987.
- Morigi, C., 2009. Benthic environmental changes in the Eastern Mediterranean Sea during sapropel S5 deposition. Palaeogeogr. Palaeoclimatol. Palaeoecol. 273 (3–4), 258–271. https://doi.org/10.1016/j.palaeo.2008.10.010.
- Müller, P.J., Suess, E., 1979. Productivity, sedimentation rate, and sedimentary organic matter in the oceans-I. Organic carbon preservation. Deep Sea Res. A Oceanogr. Res. Pap. 26 (12), 1347–1362. https://doi.org/10.1016/0198-0149(79)90003-7.
- Naidu, P.D., Malmgren, B.A., 1995. Do benthic foraminifer records represent a productivity index in oxygen minimum zone areas? An evaluation from the Oman Margin, Arabian Sea. Mar. Micropaleontol. 26 (1–4), 49–55. https://doi.org/ 10.1016/0377-8398(95)00014-3.
- Nicholls, K.W., Østerhus, S., Makinson, K., Gammelsrød, T., Fahrbach, E., 2009. Ice-ocean processes over the continental shelf of the southern Weddell Sea, Antarctica: a review. Rev. Geophys. 47 (3) https://doi.org/10.1029/2007RG000250.
- Nowlin, W.D., Klinck, J.M., 1986. The physics of the Antarctic Circumpolar Current. Rev. Geophys. 24 (3), 469–491. https://doi.org/10.1029/RG024i003p00469.
- Olóriz, F., Reolid, M., Rodríguez-Tovar, F.J., 2012. Palaeogeography and relative sealevel history forcing eco-sedimentary contexts in Late Jurassic epicontinental shelves (Prebetic Zone, Betic Cordillera): an ecostratigraphic approach. Earth Sci. Rev. 111 (1–2), 154–178. https://doi.org/10.1016/j.earscirev.2011.11.004.
- Orsi, A.H., Wiederwohl, C.L., 2009. A recount of Ross Sea waters. Deep-Sea Res. II Top. Stud. Oceanogr. 56 (13–14), 778–795. https://doi.org/10.1016/j.dsr2.2008.10.033.
- Orsi, A.H., Whitworth, T., Nowlin, W.D., 1995. On the meridional extent and fronts of the Antarctic Circumpolar Current. Deep-Sea Res. I Oceanogr. Res. Pap. 42 (5), 641–673. https://doi.org/10.1016/0967-0637(95)00021-W.
- Orsi, A.H., Johnson, G.C., Bullister, J.L., 1999. Circulation, mixing, and production of Antarctic Bottom Water. Prog. Oceanogr. 43 (1), 55–109. https://doi.org/10.1016/ S0079-6611(99)00004-X.
- Orsi, A.H., Smethie, W.M., Bullister, J.L., 2002. On the total input of Antarctic waters to the deep ocean: a preliminary estimate from chlorofluorocarbon measurements. J. Geophys. Res. Oceans 107 (C8). https://doi.org/10.1029/2001JC000976, 31(1-14)
- Pahnke, K., Zahn, R., 2005. Southern hemisphere water mass conversion linked with North Atlantic climate variability. Science 307 (5716), 1741–1746. https://doi.org/ 10.1126/science.1102163.
- Pérez, L.F., Martos, Y.M., García, M., Weber, M.E., Raymo, M.E., Williams, T., Zheng, X., 2021. Miocene to present oceanographic variability in the Scotia Sea and Antarctic ice sheets dynamics: insight from revised seismic-stratigraphy following IODP

- expedition 382. Earth Planet. Sci. Lett. 553, 116657 https://doi.org/10.1016/j.
- Pérez-Asensio, J.N., Aguirre, J., Rodríguez-Tovar, F.J., 2017. The effect of bioturbation by polychaetes (Opheliidae) on benthic foraminiferal assemblages and test preservation. Palaeontology 60 (6), 807–827. https://doi.org/10.1111/pala.12317.
- Phillips, R., Xu, J., 2021. A critical review of molybdenum sequestration mechanisms under euxinic conditions: implications for the precision of molybdenum paleoredox proxies. Earth-Sci. Rev. 221, 103799 https://doi.org/10.1016/j. earscirev.2021.103799.
- Pillot, Q., Suchéras-Marx, B., Sarr, A.C., Bolton, C.T., Donnadieu, Y., 2023. A global reassessment of the spatial and temporal expression of the Late Miocene biogenic bloom. Paleoceanogr. Paleoclimatol. 38 (3) https://doi.org/10.1029/ 2022PA004564 e2022PA004564.
- Pound, M.J., Haywood, A.M., Salzmann, U., Riding, J.B., Lunt, D.J., Hunter, S.J., 2011. A Tortonian (Late Miocene, 11.61–7.25 Ma) global vegetation reconstruction. Palaeogeogr. Palaeoclimatol. Palaeoecol. 300 (1–4), 29–45. https://doi.org/ 10.1016/J.PALAEO.2010.11.029.
- Prescott, C.L., Haywood, A.M., Dolan, A.M., Hunter, S.J., Tindall, J.C., 2019. Indian monsoon variability in response to orbital forcing during the late Pliocene. Glob. Planet. Chang. 173, 33–46. https://doi.org/10.1016/j.gloplacha.2018.12.002.
- Rathburn, A.E., Corliss, B.H., 1994. The ecology of living (stained) deep-sea benthic foraminifera from the Sulu Sea. Paleoceanography 9 (1), 87–150. https://doi.org/ 10.1029/93PA02327
- Rintoul, S.R., Hughes, C.W., Olbers, D., 2001. Chapter 4.6 The Antarctic Circumpolar Current system. In: International Geophysics, 77, pp. 271–302. XXIX - XXXVI. https://doi.org/10.1016/S0074-6142(01)80124-8.
- https://doi.org/10.1016/S0074-6142(01)80124-8.

 Schiebel, R., Hemleben, C., 2017. Planktic Foraminifers in the Modern Ocean. Springer, Berlin, Heidelberg, XVII, p. 358. https://doi.org/10.1007/978-3-662-50297-6.
- Schmiedl, G., Mackensen, A., 1997. Late Quaternary paleoproductivity and deep water circulation in the eastern South Atlantic Ocean: evidence from benthic foraminifera. Palaeogeogr. Palaeoclimatol. Palaeoecol. 130 (1–4), 43–80. https://doi.org/ 10.1016/S0031-0182(96)00137-X.
- Schmiedl, G., Mackensen, A., Müller, P.J., 1997. Recent benthic foraminifera from the eastern South Atlantic Ocean: dependence on food supply and water masses. Mar. Micropaleontol. 32 (3–4), 249–287. https://doi.org/10.1016/S0377-8398(97) 00023-6.
- Schmiedl, G., De Bovée, F., Buscail, R., Charrière, B., Hemleben, C., Medernach, L., Picon, P., 2000. Trophic control of benthic foraminiferal abundance and microhabitat in the bathyal Gulf of Lions, western Mediterranean Sea. Mar. Micropaleontol. 40 (3), 167–188. https://doi.org/10.1016/S0377-8398(00)00038-4
- Scott, D.B., Takayanagi, Y., Hasegawa, S., Saito, T., 2000. Illustration and taxonomic reevaluation of neogene foraminifera described from Japan. Palaeontol. Electron. 3 (2), 1–41. https://palaeo-electronica.org/2000 2/foram/foram.pdf.
- Sigman, D.M., Hain, M.P., Haug, G.H., 2010. The polar ocean and glacial cycles in atmospheric CO₂ concentration. Nature 466 (7302), 47–55. https://doi.org/ 10.1038/nature09149.
- Singh, R.K., Gupta, A.K., 2004. Late Oligocene–Miocene paleoceanographic evolution of the southeastern Indian Ocean: evidence from deep-sea benthic foraminifera (ODP Site 757). Mar. Micropaleontol. 51 (1–2), 153–170. https://doi.org/10.1016/j. marmicro.2003.10.003
- Singh, R.K., Gupta, A.K., 2010. Deep-sea benthic foraminiferal changes in the eastern Indian Ocean (ODP Hole 757B): their links to deep Indonesian (Pacific) flow and high latitude glaciation during the Neogene. Episodes 33 (2), 74–82. https://doi. org/10.18814/epiiugs/2010/v33i2/001.
- Singh, R.K., Gupta, A.K., Das, M., 2012. Paleoceanographic significance of deep-sea benthic foraminiferal species diversity at southeastern Indian Ocean Hole 752A during the Neogene. Palaeogeogr. Palaeoclimatol. Palaeoecol. 361–362, 94–103. https://doi.org/10.1016/j.palaeo.2012.08.008.
- Singh, R.K., Gupta, A.K., Das, M., Flower, B.P., 2021. Paleoceanographic turnovers during the Plio-Pleistocene in the southeastern Indian Ocean: linkages with Northern Hemisphere glaciation and Indian monsoon variability. Palaeogeogr. Palaeoclimatol. Palaeoecol. 571, 110374 https://doi.org/10.1016/j.palaeo.2021.110374.
- Skinner, L.C., Fallon, S., Waelbroeck, C., Michel, E., Barker, S., 2010. Ventilation of the deep southern ocean and deglacial CO₂ rise. Science 328 (5982), 1147–1151. https://doi.org/10.1126/science.1183627.
- Sloyan, B.M., Rintoul, S.R., 2001. Circulation, renewal, and modification of Antarctic mode and intermediate water. J. Phys. Oceanogr. 31 (4), 1005–1030. https://doi. org/10.1175/1520-0485(2001)031<1005:CRAMOA>2.0.CO;2.
- Smart, C.W., Thomas, E., Ramsay, A.T.S., 2007. Middle-late Miocene benthic foraminifera in a western equatorial Indian Ocean depth transect: paleoceanographic implications. Palaeogeogr. Palaeoclimatol. Palaeoecol. 247 (3–4), 402–420. https://doi.org/10.1016/j.palaeo.2006.11.003.

- Speer, K., Rintoul, S.R., Sloyan, B., 2000. The diabatic Deacon cell. J. Phys. Oceanogr. 30 (12), 3212–3222. https://doi.org/10.1175/1520-0485(2000)030<3212:TDDC>2.0.
- Steinthorsdottir, M., Coxall, H.K., de Boer, A.M., Huber, M., Barbolini, N., Bradshaw, C. D., Burls, N.J., Feakins, S.J., Gasson, E., Henderiks, J., Holbourn, A.E., Kiel, S., Kohn, M.J., Knorr, G., Kürschner, W.M., Lear, C.H., Liebrand, D., Lunt, D.J., Mörs, T., Strömberg, C.A.E., 2021. The Miocene: the future of the past. Paleoceanogr. Paleoclimatol. 36 (4) https://doi.org/10.1029/2020PA004037.
- Stommel, H., 1958. The circulation of the abyss. Sci. Am. 199 (1), 85–93. https://www.jstor.org/stable/24941060.
- Takata, H., Kim, H.J., Asahi, H., Thomas, E., Yoo, C.M., Chi, S.B., Khim, B.K., 2019. Central Equatorial Pacific benthic foraminifera during the mid-Brunhes dissolution interval: ballasting of particulate organic matter by biogenic silica and carbonate. Quat. Sci. Rev. 210, 64–79. https://doi.org/10.1016/j.quascirev.2019.02.030.
- Talley, L.D., 2013. Closure of the global overturning circulation through the Indian, Pacific, and Southern Oceans: schematics and transports. Oceanography 26 (1), 80–97. https://www.jstor.org/stable/24862019.
- Tapia, R., Ho, S.L., Núñez-Ricardo, S., Marchant, M., Lamy, F., Hebbeln, D., 2021. Increased marine productivity in the southern Humboldt current system during MIS 2–4 and 10–11. Paleoceanogr. Paleoclimatol. 36 (4) https://doi.org/10.1029/ 2020PA004066 e2020PA004066.
- Thena, T., Mohan, K., Prakasam, M., Saravanan, K., 2021. Palaeoecological significances of deep-sea benthic foraminifera from Cascadia Margin, North East Pacific Ocean. Reg. Stud. Mar. Sci. 47, 101949 https://doi.org/10.1016/j.rsma.2021.101949.
- Toyos, M.H., Lamy, F., Lange, C.B., Lembke-Jene, L., Saavedra-Pellitero, M., Esper, O., Arz, H.W., 2020. Antarctic Circumpolar Current dynamics at the Pacific entrance to the Drake Passage over the past 1.3 million years. Paleoceanogr. Paleoclimatol. 35 (7) https://doi.org/10.1029/2019PA003773 e2019PA003773.
- Vats, N., Singh, R.K., Das, M., Holbourn, A., Gupta, A.K., Gallagher, S.J., Pandey, D.K., 2021. Linkages between East China Sea deep-sea oxygenation and variability in the East Asian summer monsoon and Kuroshio current over the last 400,000 years. Paleoceanogr. Paleoclimatol. 36 (12) https://doi.org/10.1029/2021PA004261.
- Verma, S., Gupta, A.K., Singh, R.K., 2013. Variations in deep-sea benthic foraminifera at ODP Hole 756B, southeastern Indian Ocean: evidence for changes in deep ocean circulation. Palaeogeogr. Palaeoclimatol. Palaeoecol. 376, 172–183. https://doi.org/ 10.1016/j.palaeo.2013.02.034.
- Warren, B.A., 1981. Transindian hydrographic section at lat. 18 degree s: property distributions and circulation in the south indian ocean. Deep-Sea Res. A Oceanogr. Res. Pap. 28 (8 A Pt A), 759–788. https://doi.org/10.1016/s0198-0149(81)80001-5.
- Wellner, J.S., Gohl, K., Klaus, A., Bauersachs, T., Bohaty, S.M., Courtillat, M., Cowan, E. A., De Lira Mota, M.A., Esteves, M.S.R., Fegyveresi, J.M., Frederichs, T., Gao, L., Halberstadt, A.R., Hillenbrand, C.-D., Horikawa, K., Iwai, M., Kim, J.-H., King, T.M., Klages, J.P., Passchier, S., Penkrot, M.L., Prebble, J.G., Rahaman, W., Reinardy, B.T. I., Renaudie, J., Robinson, D.E., Scherer, R.P., Siddoway, C.S., Wu, L., Yamane, M., 2021. Site U1532. In: Gohl, K., Wellner, J.S., Klaus, A., the Expedition 379 Scientists (Eds.), Amundsen Sea West Antarctic Ice Sheet History. Proceedings of the International Ocean Discovery Program, 379: College Station, TX (International Ocean Discovery Program). https://doi.org/10.14379/iodp.proc.379.103.2021.
- Winckler, G., Lamy, F., Alvarez Zarikian, C.A., Arz, H.W., Basak, C., Brombacher, A., Esper, O.M., Farmer, J.R., Gottschalk, J., Herbert, L.C., Iwasaki, S., Lawson, V.J., Lembke-Jene, L., Lo, L., Malinverno, E., Michel, E., Middleton, J.L., Moretti, S., Moy, C.M., Foucher McColl, N., 2021. Site U1541. https://doi.org/10.14379/iodp.proc.383.105.2021.
- Wu, S., Lembke-Jene, L., Lamy, F., Arz, H.W., Nowaczyk, N., Xiao, W., Zhang, X., Hass, H.C., Titschack, J., Zheng, X., Liu, J., Dumm, L., Diekmann, B., Nürnberg, D., Tiedemann, R., Kuhn, G., 2021. Orbital- and millennial-scale Antarctic Circumpolar Current variability in Drake Passage over the past 140,000 years. Nat. Commun. 12 (1) https://doi.org/10.1038/s41467-021-24264-9.
- Yasuhara, M., Cronin, T.M., Hunt, G., Hodell, D.A., 2009. Deep-sea ostracods from the South Atlantic sector of the Southern Ocean during the last 370,000 years. J. Paleontol. 83 (6), 914–930. https://doi.org/10.1666/08-149.1.
- Yin, Q., 2013. Insolation-induced mid-Brunhes transition in Southern Ocean ventilation and deep-ocean temperature. Nature 494 (7436), 222–225. https://doi.org/ 10.1038/nature11790.
- Zhang, C., Dang, H., Azam, F., Benner, R., Legendre, L., Passow, U., Polimene, L., Robinson, C., Suttle, C.A., Jiao, N., 2018. Evolving paradigms in biological carbon cycling in the ocean. Natl. Sci. Rev. 5 (4), 481–499. https://doi.org/10.1093/nsr/ nwv074.
- Zweng, M.M., Reagan, J.R., Seidov, D., Boyer, T.P., Locarnini, R.A., Garcia, H.E., Mishonov, A.V., Baranova, O.K., Weathers, K.W., Paver, C.R., Smolyar, I.V., 2019. World Ocean Atlas 2018, Volume 2: Salinity. A. Mishonov, Technical Editor, NOAA Atlas NESDIS 82, p. 50. https://data.nodc.noaa.gov/woa/WOA18/DOC/woa18_vol2.pdf.